The Cumulant Theory of Cyclostationary Time-Series, Part II: Development and Applications

Chad M. Spooner, *Member, IEEE,* and William A. Gardner, *Fellow, IEEE*

Abstract—**The development of the theory of nonlinear processing of cyclostationary time-series that is initiated in the first part of this two-part paper is continued here in the second part. A new type of cumulant for complex-valued variables is introduced and used to generalize the temporal and spectral moments and cumulants for cyclostationary time-series from real-valued to complex-valued time-series. The relations between the temporal and spectral moments and cumulants at the inputs and outputs of several signal processing operations are determined. Formulas for the temporal and spectral cumulants of complex-valued pulse-amplitude-modulated time-series are derived. Estimators for the temporal moments and cumulants and for the cyclic polyspectra are presented and their properties are discussed. The performance of these estimators is illustrated by several computer simulation examples for pulse-amplitude-modulated time-series. The theory is applied to the problems of weak-signal detection and interference-tolerant time-delay estimation.**

I. Introduction

THIS sequel to [34] (herein referred to as Part I, which is also in this issue) continues the development of the theory of nonlinear processing of cyclostationary time-series. It also applies this theory to the problems of weak-signal detection and interference-tolerant time-delay estimation. A cyclostationary time-series is one from which finite-strength additive sine waves can be generated by using nonlinear transformations, but which typically does not itself contain finite-strength additive sine-wave components. The minimum order of nonlinearity that is required to generate a sine wave is called the *order of cyclostationarity* of the time-series, and the frequency of a regenerated sine wave is called a *cycle frequency*. For example, a suppressed-carrier amplitude-modulated time-series is second-order cyclostationary because a sine wave with frequency equal to twice the carrier frequency can be generated by using a squarer. As another example, a pulse-amplitude-modulated (PAM) time-series with positive-frequency bandwidth equal to half the pulse rate is fourth-order cyclostationary because no nonlinearities of order less than four can generate a sine wave from such a time-series, but a fourth-order nonlinearity can generate a sine wave with frequency equal to the pulse rate.

The theory of second-order cyclostationary time-series (or second-order cyclostationarity (SOCS)) has been developed over the last decade [10], [11], and has found application to numerous signal processing problems, such as weak-signal detection, time-delay estimation, interference removal, system identification, direction finding, and blind-adaptive spatial filtering (see references in Part I and in [14]). The exploitation of SOCS is particularly beneficial when the time-series of interest is heavily corrupted by (stationary or nonstationary) noise and interference. This is so because the SOCS parameters associated with a particular cycle frequency α of such a time-series can, in principle, be reliably extracted regardless of the amount and type of interference, provided only that neither the noise nor the interference exhibit SOCS with the same cycle frequency α. This last requirement typically means that the time-series of interest must have a unique symbol rate, chip rate, hop rate, frame rate, carrier frequency, or frequency associated with some other underlying periodicity.

In order to take advantage of this property of tolerance to noise and interference for time-series that are cyclostationary of order $n > 2$, it is necessary to generalize the theory of SOCS to a theory of higher order cyclostationarity (HOCS). The motivation and foundation for this generalization is given in the first part of this two-part paper. Before continuing the development of the theory, the key definitions and concepts from Part I are summarized.

Following the summary of Part I in Section II, the parameters of HOCS are generalized from real-valued time-series to complex-valued time-series in Section III, and in Section IV the effects of signal processing operations on the parameters of HOCS are determined. The temporal and spectral parameters are calculated for a complex-valued PAM time-series model in Section V, measurement techniques are discussed in Section VI, and in Section VII the theory is applied to the problems of weak-signal detection and time-delay estimation. Conclusions are drawn in Section VIII.

Manuscript received April 2, 1992; revised April 26, 1994. This work was supported by the National Science Foundation under Grants MIP-88-12902 and MIP-91-12800, the United States Army Research Office under contract DAAL03-91-C-0018; and E-Systems, Inc. (Greenville Division). The associate editor coordinating the review of this paper and approving it for publication was Prof. José A. R. Fonollosa.

C. M. Spooner is with Mission Research Corporation, Monterey, CA 93940 USA.

W. A. Gardner is with the Department of Electrical and Computer Engineering, University of California, Davis, CA 95616 USA.

IEEE Log Number 9406034.

II. Key Definitions and Concepts from Part I

A. Analysis Framework

The analysis framework that is used in this paper is the fraction-of-time (FOT) probabilistic framework, wherein the usual expectation operation $E\{\cdot\}$ is replaced by the *sine-wave-extraction operation* $\hat{E}^{\{\alpha\}}\{\cdot\}$. The sine-wave-extraction

1053–587X/94$04.00 © 1994 IEEE

operation extracts all finite-strength additive sine-wave components from its argument, including the sine wave with frequency equal to zero (the dc component):

$$\hat{E}^{\{\alpha\}}\{g(t)\} = \sum_{\alpha} g_\alpha e^{i2\pi\alpha t} \tag{1}$$

where

$$g_\alpha \triangleq \lim_{T\to\infty} \frac{1}{T} \int_{-T/2}^{T/2} g(u) e^{-i2\pi\alpha u} du \equiv \langle g(u) e^{-i2\pi\alpha u} \rangle. \tag{2}$$

The operation $\hat{E}^{\{\alpha\}}\{\cdot\}$ is actually an expectation operation with respect to the FOT probability density function (PDF) for $g(t)$. It is argued in Part I, and in [11] and [39], that the FOT framework provides the most appropriate set of tools for developing a pragmatic theory of cyclostationary signals. However, it is not appropriate for generally nonstationary signals, since it is based on infinite-time averages. Because the FOT framework is dual to the stochastic process framework (for stationary and cyclostationary time-series), we can use all of the notation and terminology that is associated with the probabilistic theory of stochastic processes, such as moment, cumulant, and characteristic function [13], [39].

It should be emphasized that all of the results in this paper and in Part I can be understood using stochastic process theory provided only that the class of processes considered exhibits appropriate ergodicity properties. Thus, the reader can, if he or she wishes, interpret $\hat{E}^{\{\alpha\}}\{\cdot\}$ to be the familiar stochastic expectation operation. However, it should also be emphasized that by avoiding the unnecessary abstraction of ensembles that underlies the stochastic process, the FOT framework has enabled us to develop the theory in a manner that is consistent with the ideas of single-data-record measurement and application to signal processing problems involving single data records, and it has resulted in our deriving the cumulant as the solution to a practically motivated problem involving sine-wave generation (See Part I, Section II).

B. Pure nth-Order Sine Waves

Since the aim of the present study is to characterize the additive sine-wave components generated by nonlinearly transforming cyclostationary time-series, it is natural to consider the sine-wave components in nth-order lag products (elementary homogeneous nth-order polynomial transformations)

$$L_x(t,\boldsymbol{\tau})_n \triangleq \prod_{j=1}^{n} x(t+\tau_j), \quad \boldsymbol{\tau} \triangleq [\tau_1 \cdots \tau_n]^\dagger \tag{3}$$

of the time-series $x(t)$ under consideration (see Part I, Section II). For an nth-order cyclostationary time-series $x(t)$, the quantities

$$R_x^\alpha(\boldsymbol{\tau})_n \triangleq \langle L_x(t,\boldsymbol{\tau})_n e^{-i2\pi\alpha t} \rangle \tag{4}$$

for all α for which they are not identically zero completely characterize the additive sine-wave components in homogeneous nth-order polynomial transformations of $x(t)$, but if $x(t)$ also exhibits lower order cyclostationarity (order lower than n), then the lag product $L_x(t,\boldsymbol{\tau})_n$ can contain sine waves that are due to multiplication of sine waves associated with lower order lag products, namely, factors of $L_x(t,\boldsymbol{\tau})_n$. A *pure nth-order sine wave* is the sine-wave component of the nth-order lag product that is left after all products of sine waves from lower order lag products obtained by factoring the nth-order lag product have been subtracted out. In Part I, it is shown that the sum of all pure nth-order sine waves for a time-series $x(t)$ and a particular lag vector $\boldsymbol{\tau}$ is equal to the *nth-order temporal cumulant function* for $x(t)$, that is, the nth-order cumulant for the set of variables $\{x(t+\tau_j)\}_{j=1}^n$ obtained by using the FOT PDF's for $x(t)$ for orders 1 through n (Part I, Section II–B).

C. Time-Domain Parameters of HOCS

Both moments and cumulants are useful in characterizing the sine-wave components in nth-order nonlinear transformations of cyclostationary time-series; let us start with moments. The *nth-order temporal moment function* (TMF) is defined to be the temporal expected value of the nth-order lag product

$$R_x(t,\boldsymbol{\tau})_n \triangleq \hat{E}^{\{\alpha\}}\left\{\prod_{j=1}^{n} x(t+\tau_j)\right\} \equiv \hat{E}^{\{\alpha\}}\{L_x(t,\boldsymbol{\tau})_n\} \tag{5}$$

and can be expressed as

$$R_x(t,\boldsymbol{\tau})_n = \sum_{\alpha} R_x^\alpha(\boldsymbol{\tau})_n e^{i2\pi\alpha t}$$

where $R_x^\alpha(\boldsymbol{\tau})_n$ is the *nth-order cyclic temporal moment function* (CTMF), which is the lag-dependent Fourier coefficient

$$R_x^\alpha(\boldsymbol{\tau})_n = \langle R_x(t,\boldsymbol{\tau})_n e^{-i2\pi\alpha t} \rangle \tag{6}$$

and is equal to

$$R_x^\alpha(\boldsymbol{\tau})_n = \langle L_x(t,\boldsymbol{\tau})_n e^{-i2\pi\alpha t} \rangle$$

which is taken to be its definition. The *nth-order temporal cumulant function* (TCF) is given by

$$C_x(t,\boldsymbol{\tau})_n = \sum_{P_n} \left[(-1)^{p-1}(p-1)! \prod_{j=1}^{p} R_x(t,\boldsymbol{\tau}_{\nu_j})_{n_j} \right] \tag{7}$$

where the sum is over all distinct partitions P_n, such as $\{\nu_k\}_{k=1}^p$, of the index set $\{1,2,\cdots,n\}$, p is the number of elements in a partition ($1 \le p \le n$), $n_j = |\nu_j|$, and

$$R_x(t,\boldsymbol{\tau}_{\nu_j})_{n_j} \triangleq \hat{E}^{\{\alpha\}}\left\{\prod_{k\in\nu_j} x(t+\tau_k)\right\}$$

where $\boldsymbol{\tau}_{\nu_j}$ is the vector of lags in $\boldsymbol{\tau}$ with indices in ν_j. The *nth-order cyclic temporal cumulant function* (CTCF) is the Fourier coefficient of the TCF

$$C_x^\beta(\boldsymbol{\tau})_n \triangleq \langle C_x(t,\boldsymbol{\tau})_n e^{-i2\pi\beta t} \rangle \tag{8}$$

and can be expressed in terms of lower order CTMF's by using (7) in (8):

$$C_x^\beta(\boldsymbol{\tau})_n = \sum_{P_n} \left[(-1)^{p-1}(p-1)! \sum_{\boldsymbol{\alpha}^\dagger \mathbf{1}=\beta} \prod_{j=1}^{p} R_x^{\alpha_j}(\boldsymbol{\tau}_{\nu_j})_{n_j} \right]. \tag{9}$$

In (9), $\boldsymbol{\alpha}$ is a vector of p cycle frequencies $[\alpha_1 \cdots \alpha_p]$ and $\mathbf{1}$ is the vector of ones. The CTCF corresponds to the strength (magnitude and phase) of the pure nth-order sine wave with frequency β in the lag product $L_x(t,\boldsymbol{\tau})_n$. It can be shown that the nth-order TMF is related to TCF's of orders less than or equal to n by

$$R_x(t,\boldsymbol{\tau})_n = \sum_{P_n} \left[\prod_{j=1}^{p} C_x(t,\boldsymbol{\tau}_{\nu_j})_{n_j} \right] \tag{10}$$

from which

$$R_x^{\alpha}(\boldsymbol{\tau})_n = \sum_{P_n} \left[\sum_{\boldsymbol{\beta}^{\dagger}\mathbf{1}=\alpha} \prod_{j=1}^{p} C_x^{\beta_j}(\boldsymbol{\tau}_{\nu_j})_{n_j} \right] \tag{11}$$

can be deduced.

As shown in Part I, the following two reduced-dimension (RD) functions play a central role in the theory

$$\text{RD-CTMF:} \qquad \bar{R}_x^{\alpha}(\boldsymbol{u})_n \triangleq \left\langle x(t) \prod_{j=1}^{n-1} x(t+u_j) e^{-i2\pi\alpha t} \right\rangle, \quad \boldsymbol{u} = [u_1 \cdots u_{n-1}]^{\dagger} \tag{12}$$

$$\text{RD-CTCF:} \qquad \bar{C}_x^{\beta}(\boldsymbol{u})_n \triangleq C_x^{\beta}([\boldsymbol{u}\ 0])_n. \tag{13}$$

In general, the RD-CTMF is not integrable with respect to $\boldsymbol{u}$, whereas the RD-CTCF is for a large class of time-series models of practical interest, and the RD-CTCF is signal selective, whereas the RD-CTMF is not (see Part I, Section II–C). Specifically, if $x(t)$ consists of the sum of M statistically independent time-series $s_j(t)$,

$$x(t) = \sum_{j=1}^{M} s_j(t)$$

then

$$C_x(t,\boldsymbol{\tau})_n = \sum_{j=1}^{M} C_{s_j}(t,\boldsymbol{\tau})_n$$

and if β is an nth-order (pure) cycle frequency that is unique to $s_k(t)$ then

$$C_x^{\beta}(\boldsymbol{\tau})_n = C_{s_k}^{\beta}(\boldsymbol{\tau})_n.$$

D. Frequency-Domain Parameters of HOCS

The spectral parameters of HOCS are defined in Part I in terms of the complex envelopes

$$X_T(t,f) \triangleq \int_{t-T/2}^{t+T/2} x(v) e^{-i2\pi f v} dv \tag{14}$$

of narrowband spectral components of the time-series $x(t)$ at n frequencies. The spectral parameters are characterized by the Fourier transforms of the temporal parameters, as is evident in the following summary. The *nth-order spectral moment function* (SMF) is defined by

$$S_x(\boldsymbol{f})_n \triangleq \lim_{T\to\infty} S_{x_T}(\boldsymbol{f})_n \triangleq \lim_{T\to\infty} \left\langle \prod_{j=1}^{n} X_T(t,f_j) \right\rangle, \quad \boldsymbol{f} = [f_1 \cdots f_n]^{\dagger} \tag{15}$$

and can be expressed as

$$S_x(\boldsymbol{f})_n = \sum_{\alpha} \bar{S}_x^{\alpha}(\boldsymbol{f}')_n \delta(\boldsymbol{f}^{\dagger}\mathbf{1} - \alpha), \quad \boldsymbol{f}' = [f_1 \cdots f_{n-1}]^{\dagger} \tag{16}$$

where $\bar{S}_x^{\alpha}(\boldsymbol{f}')_n$ is the *nth-order reduced-dimension spectral moment function* (RD-SMF)

$$\bar{S}_x^{\alpha}(\boldsymbol{f}')_n \triangleq \mathcal{F}^{n-1}\{\bar{R}_x^{\alpha}(\boldsymbol{u})_n\} \tag{17}$$

in which $\mathcal{F}^{n-1}$ denotes $(n-1)$th-order Fourier transformation. The *nth-order spectral cumulant function* (SCF) is defined by

$$P_x(\boldsymbol{f})_n \triangleq \lim_{T\to\infty} P_{x_T}(\boldsymbol{f})_n \triangleq \lim_{T\to\infty} \sum_{P_n} \left[(-1)^{p-1}(p-1)! \prod_{j=1}^{p} S_{x_T}(\boldsymbol{f}_{\nu_j})_{n_j} \right] \tag{18}$$

and can be expressed as

$$P_x(\boldsymbol{f})_n = \sum_{\beta} \bar{P}_x^{\beta}(\boldsymbol{f}')_n \delta(\boldsymbol{f}^{\dagger}\mathbf{1} - \beta) \tag{19}$$

where $\bar{P}_x^{\beta}(\boldsymbol{f}')_n$ is the *nth-order cyclic polyspectrum* (CP), which is defined by

$$\bar{P}_x^{\beta}(\boldsymbol{f}')_n \triangleq \mathcal{F}^{n-1}\{\bar{C}_x^{\beta}(\boldsymbol{u})_n\}. \tag{20}$$

In (18), the vector of frequencies $\boldsymbol{f}_{\nu_j}$ consists of the elements of $\boldsymbol{f}$ with indices in the partition element ν_j. The following formal relations are useful in subsequent sections of the paper:

$$\mathcal{F}^n\{R_x^{\alpha}(\boldsymbol{\tau})_n\} = \bar{S}_x^{\alpha}(\boldsymbol{f}')_n \delta(\boldsymbol{f}^{\dagger}\mathbf{1} - \alpha) \tag{21}$$

$$\mathcal{F}^n\{C_x^{\beta}(\boldsymbol{\tau})_n\} = \bar{P}_x^{\beta}(\boldsymbol{f}')_n \delta(\boldsymbol{f}^{\dagger}\mathbf{1} - \beta). \tag{22}$$

The CP is the only generally well-behaved spectral characterization of HOCS; the other functions are typically impulsive, and can even contain products of impulses. For a time-series $x(t)$ that is stationary of order n, we have $\bar{P}_x^{\beta}(\boldsymbol{f}')_m \equiv 0$ for $\beta \neq 0$ and $m \leq n$. If $x(t)$ can be viewed as a sample path of a cycloergodic stationary stochastic process, then $\bar{P}_x^{0}(\boldsymbol{f}')_n$ is equivalent (with probability one) to the conventional nth-order polyspectrum for the process [1]-[3], [26], [27], [29]. However, if the cycloergodicity assumption does not hold, then the CP $\bar{P}_x^{0}(\boldsymbol{f}')_n$ can differ from the polyspectrum for the process for almost every sample path. In this case, both parameters are well-defined, but single-record estimation of the polyspectrum for the stochastic process is not possible. A common way to (inadvertently or otherwise) destroy cycloergodicity is to phase-randomize a process. By introducing random phase variables into a stochastic model, a stationary process can be obtained that has cyclostationary sample paths. This is illustrated with a numerical example in Section VI–C (other examples are given in [39]).

III. Complex-Valued Time-Series

To allow for arbitrary conjugations in the lag product of a complex-valued time-series $x(t)$, we use the notation

$$L_x(t,\boldsymbol{\tau})_n = \prod_{j=1}^{n} x^{(*)_j}(t+\tau_j) \tag{23}$$

where $(*)_j$ is either a conjugation $*$ or nothing, that is, $(*)_j$ is an optional conjugation of the jth factor $x(t+\tau_j)$. For *each* of the 2^n different choices of conjugations in (23) we define the CTMF by

$$R_x^\alpha(\boldsymbol{\tau})_n \triangleq \langle L_x(t,\boldsymbol{\tau})_n e^{-i2\pi\alpha t}\rangle$$

and its reduced-dimension counterpart by

$$\bar{R}_x^\alpha(\boldsymbol{u})_n \triangleq R_x^\alpha(\boldsymbol{\tau})_n \text{ for } \tau_n = 0 \text{ and } \tau_j = u_j \text{ for } 1 \le j \le n-1$$

as in Part I for real time-series. The chosen notation does not indicate the number or placement of the optional conjugations. This is done to avoid further complications to an already complicated notation.

In general, the 2^n functions $R_x^\alpha(\boldsymbol{\tau})_n$ are distinct. This is immediately clear in the case of $n = 2$, where we have

$$\begin{aligned}
R_{x_1}^\alpha(\boldsymbol{\tau})_2 &= \langle x(t+\tau_1)x(t+\tau_2)e^{-i2\pi\alpha t}\rangle,\\
R_{x_2}^\alpha(\boldsymbol{\tau})_2 &= \langle x^*(t+\tau_1)x(t+\tau_2)e^{-i2\pi\alpha t}\rangle,\\
R_{x_3}^\alpha(\boldsymbol{\tau})_2 &= \langle x(t+\tau_1)x^*(t+\tau_2)e^{-i2\pi\alpha t}\rangle,\\
R_{x_4}^\alpha(\boldsymbol{\tau})_2 &= \langle x^*(t+\tau_1)x^*(t+\tau_2)e^{-i2\pi\alpha t}\rangle.
\end{aligned}$$

For real time-series these four functions are equivalent. For complex-valued time-series they are not and, instead, the following relations hold:

$$\begin{aligned}
R_{x_1}^\alpha(\tau_1,\tau_2)_2 &= R_{x_4}^{-\alpha}(\tau_1,\tau_2)_2^*\\
R_{x_2}^\alpha(\tau_1,\tau_2)_2 &= R_{x_3}^{-\alpha}(\tau_1,\tau_2)_2^*.
\end{aligned}$$

For certain complex-valued signal types and certain values of n, the cycle frequency sets that are associated with some choices of conjugations can be disjoint, as illustrated in [11] for the case of n =2. For many complex-valued communication signal models, the choice of no conjugations yields cycle frequencies that are related to the carrier frequency (or carrier offset), whereas the choice of $n/2$ conjugations (for n even) yields cycle frequencies related to the pulse rate.

For an arbitrary collection of time-series translates $\{y_i(t+\tau_i)\}_{i=1}^n$, the cross (or joint) CTMF is defined by

$$R_y^\alpha(\boldsymbol{\tau})_n = \left\langle \prod_{j=1}^n y_j(t+\tau_j)e^{-i2\pi\alpha t}\right\rangle \tag{24}$$

and the cross SMF is given by

$$S_y(\boldsymbol{f})_n = \lim_{T\to\infty}\left\langle \prod_{j=1}^n Y_{jT}(t,f_j)\right\rangle. \tag{25}$$

By analogy with the analysis in Section III of Part I for real-valued time-series, (25) is not identically zero only if $\boldsymbol{f}^\dagger\mathbf{1} = \sum_{j=1}^n f_j = \alpha$, where α is an nth-order cycle frequency of $\{y_j(t)\}_{j=1}^n$ (i.e., only if (24) is not identically zero as a function of $\boldsymbol{\tau}$ for this α), in which case (25) is the n-dimensional Fourier transform of (24). Choosing $y_j(t+\tau_j) = x^{(*)_j}(t+\tau_j)$, we obtain

$$\begin{aligned}
Y_{jT}(t,f_j) &= \int_{t-T/2}^{t+T/2} x^{(*)_j}(u)e^{-i2\pi f_j u}du\\
&= \left[\int_{t-T/2}^{t+T/2} x(u)e^{-i2\pi(-)_j f_j u}du\right]^{(*)_j}\\
&= X_T^{(*)_j}(t,(-)_j f_j)
\end{aligned}$$

where $(-)_j$ is the optional minus sign associated with the optional conjugation $(*)_j$. We can express the SMF for $\{y_i(t+\tau_i)\}$ in terms of $X_T(t,f)$ by

$$S_y(\boldsymbol{f})_n = \lim_{T\to\infty}\left\langle \prod_{j=1}^n X_T^{(*)_j}(t,(-)_j f_j)\right\rangle \tag{26}$$

which is not identically zero only if $\boldsymbol{f}^\dagger\mathbf{1} = \alpha$, where α is an nth-order cycle frequency for the set $\{x^{(*)_j}(t+\tau_j)\}_{j=1}^n$.

We can construct the RD-CTCF in the same manner as in Part I for real-valued time-series, that is, by combining lower order CTMF's. However, this requires the introduction of a new type of cumulant for complex-valued variables, as explained in Appendix A. The CP is the $(n-1)$-dimensional Fourier transform of the RD-CTCF, and is not identically zero only if $\boldsymbol{f}^\dagger\mathbf{1} = \beta$ where β is a pure nth-order cycle frequency for $\{x^{(*)_j}(t+\tau_j)\}_{j=1}^n$. Just as in the case of the SMF (26), the SCF can be thought of as the limit (as $T\to\infty$) of the joint simple cumulant of the set $\{Y_{jT}(t,f_j)\}_{j=1}^n$. Thus, the CP for the set $\{x^{(*)_j}(t+\tau_j)\}_{j=1}^n$ is characterized by the limit (as $T\to\infty$) of the cumulant of the set $\{X_T^{(*)_j}(t,(-)_j f_j)\}_{j=1}^n$, analogous to the characterization for real-valued time-series in Part I, Section III.

IV. Signal Processing Operations

In this section, we obtain input-output relations for the higher order moments and cumulants of time-series subjected to various signal processing operations, including addition, multiplication, periodic time-sampling, and convolution. The derived relations can be useful in the calculation of higher order parameters of modulated signals if such signals can be represented as a series of operations on a simpler signal for which the higher order parameters are known or can be easily determined.

A. Addition

Let $z(t)$ be equal to the sum of two statistically independent time-series $x(t)$ and $y(t)$

$$z(t) = x(t) + y(t).$$

In this case, the TCF for $z(t)$ is given by (cf. Part I, Section II)

$$C_z(t,\boldsymbol{\tau})_n = C_x(t,\boldsymbol{\tau})_n + C_y(t,\boldsymbol{\tau})_n$$

which implies that the CTCF is given by

$$C_z^\beta(\boldsymbol{\tau})_n = C_x^\beta(\boldsymbol{\tau})_n + C_y^\beta(\boldsymbol{\tau})_n$$

and that the RD-CTCF is given by

$$\bar{C}_z^{\beta}(\boldsymbol{u})_n = \bar{C}_x^{\beta}(\boldsymbol{u})_n + \bar{C}_y^{\beta}(\boldsymbol{u})_n.$$

The CP is, therefore, given by

$$\bar{P}_z^{\beta}(\boldsymbol{f}')_n = \bar{P}_x^{\beta}(\boldsymbol{f}')_n + \bar{P}_y^{\beta}(\boldsymbol{f}')_n. \tag{27}$$

No equally simple additive relations hold in general for the CTMF and SMF. The result (27) can be extended by induction to the case in which $z(t)$ consists of the sum of M statistically independent time-series.

B. Product Modulation

Let the time-series $z(t)$ be the product of two statistically independent time-series $x(t)$ and $y(t)$

$$z(t) = x(t)y(t).$$

The statistical independence ([11], [13], Section I of Part I) of $x(t)$ and $y(t)$ implies that

$$\begin{aligned}\hat{E}^{\{\alpha\}}&\left\{\prod_{j=1}^{n} x^{(*)_j}(t+\tau_j)\prod_{k=1}^{m} y^{(*)k}(t+v_k)\right\}\\ &= \hat{E}^{\{\alpha\}}\left\{\prod_{j=1}^{n} x^{(*)_j}(t+\tau_j)\right\}\\ &\quad\times \hat{E}^{\{\alpha\}}\left\{\prod_{k=1}^{m} y^{(*)k}(t+v_k)\right\}\end{aligned}$$

for all values of $n, m, \boldsymbol{\tau}$, and $\boldsymbol{v}$. The TMF (5) for $z(t)$ is therefore given by

$$\begin{aligned}R_z(t,\boldsymbol{\tau})_n &= \hat{E}^{\{\alpha\}}\left\{\prod_{j=1}^{n} z^{(*)_j}(t+\tau_j)\right\}\\ &= \hat{E}^{\{\alpha\}}\left\{\prod_{j=1}^{n} x^{(*)_j}(t+\tau_j)y^{(*)_j}(t+\tau_j)\right\}\\ &= R_x(t,\boldsymbol{\tau})_n R_y(t,\boldsymbol{\tau})_n.\end{aligned}$$

Using (10), we can represent the TMF in terms of CTMF's

$$\begin{aligned}R_z(t,\boldsymbol{\tau})_n &= \sum_{\alpha} R_z^{\alpha}(\boldsymbol{\tau})_n e^{i2\pi\alpha t}\\ &= \left[\sum_{\eta} R_x^{\eta}(\boldsymbol{\tau})_n e^{i2\pi\eta t}\right]\left[\sum_{\gamma} R_y^{\gamma}(\boldsymbol{\tau})_n e^{i2\pi\gamma t}\right]\end{aligned}$$

which implies that the CTMF for $\{z(t+\tau_j)\}_{j=1}^n$ is given by

$$\begin{aligned}R_z^{\alpha}(\boldsymbol{\tau})_n &= \langle R_z(t,\boldsymbol{\tau})_n e^{-i2\pi\alpha t}\rangle\\ &= \sum_{\eta} R_x^{\eta}(\boldsymbol{\tau})_n R_y^{\alpha-\eta}(\boldsymbol{\tau})_n \qquad (28)\\ &= \sum_{\gamma} R_x^{\alpha-\gamma}(\boldsymbol{\tau})_n R_y^{\gamma}(\boldsymbol{\tau})_n \qquad (29)\end{aligned}$$

which is a discrete convolution, where $\alpha-\eta$ is equal to only nth-order cycle frequencies for $y(t)$ in (28), and $\alpha-\gamma$ is equal to only nth-order cycle frequencies for $x(t)$ in (29). The TCF and CTCF for $\{z(t+\tau_j)\}_{j=1}^n$ can be constructed by using (7), (8), and (28) or (29). The SMF can be obtained from (28) using the convolution theorem for the Fourier transform

$$S_z^{\alpha}(\boldsymbol{f})_n = \sum_{\gamma}\int_{-\infty}^{\infty}\cdots\int_{-\infty}^{\infty} S_x^{\alpha-\gamma}(\boldsymbol{f}-\boldsymbol{g})_n S_y^{\gamma}(\boldsymbol{g})_n d\boldsymbol{g} \tag{30}$$

which is a joint continuous and discrete convolution. No equally simple input-output relations hold for the CTCF and CP if both $x(t)$ and $y(t)$ are random. If one of these time-series, say $x(t)$, is nonrandom (which in the FOT framework means it is constant, periodic, or polyperiodic [11], [13]), then its lag product is identically equal to its TMF

$$R_x(t,\boldsymbol{\tau})_n = \hat{E}^{\{\alpha\}}\{L_x(t,\boldsymbol{\tau})_n\} \equiv L_x(t,\boldsymbol{\tau})_n.$$

In this case, there is a simple formula for the temporal and spectral moments and cumulants for $z(t)$:

$$\begin{aligned}C_z(t,\boldsymbol{\tau})_n &= \sum_{P_n}\left[(-1)^{p-1}(p-1)!\prod_{j=1}^{p} R_z(t,\boldsymbol{\tau}_{\nu_j})_{n_j}\right]\\ &= \sum_{P_n}\left[(-1)^{p-1}(p-1)!\left\{\prod_{j=1}^{p} R_x(t,\boldsymbol{\tau}_{\nu_j})_{n_j}\right\}\right.\\ &\quad\left.\times\left\{\prod_{k=1}^{p} R_y(t,\boldsymbol{\tau}_{\nu_k})_{n_k}\right\}\right].\end{aligned}$$

Because $x(t)$ is nonrandom, the product of lower order TMF's for $x(t)$ is equal to the nth-order TMF for $x(t)$ for every partition and can, therefore, be factored out of the sum

$$C_z(t,\boldsymbol{\tau})_n = L_x(t,\boldsymbol{\tau})_n C_y(t,\boldsymbol{\tau})_n = R_x(t,\boldsymbol{\tau})_n C_y(t,\boldsymbol{\tau})_n.$$

Thus, in the special case where $x(t)$ is nonrandom (constant, periodic, or polyperiodic), the formulas (28)–(30) hold with $R_z, \bar{S}_z, R_y, \bar{S}_y$ replaced by $C_z, \bar{P}_z, C_y, \bar{P}_y$, respectively.

C. Linear Time-Invariant Filtering

Let $z(t)$ be equal to a filtered version of $x(t)$

$$z(t) = \int_{-\infty}^{\infty} h(\lambda)x(t-\lambda)d\lambda$$

where the impulse-response function $h(\cdot)$ is assumed to be absolutely integrable. It is easy to show that the CTMF for $\{z(t+\tau_j)\}_{j=1}^n$ is given by

$$\begin{aligned}R_z^{\alpha}(\boldsymbol{\tau})_n &= \int_{-\infty}^{\infty}\cdots\int_{-\infty}^{\infty}\left[\prod_{j=1}^{n} h^{(*)_j}(\lambda_k)\right] R_x^{\alpha}(\boldsymbol{\tau}-\boldsymbol{\lambda})_n d\boldsymbol{\lambda},\\ &\boldsymbol{\lambda} \triangleq [\lambda_1\cdots\lambda_n]^{\dagger}.\end{aligned}$$

Assuming that it exists, the SMF can be obtained by using the convolution theorem for the Fourier transform and is given by

$$S_z(\boldsymbol{f})_n = \left[\prod_{j=1}^{n} H^{(*)_j}((-)_j f_j)\right] S_x(\boldsymbol{f})_n \tag{31}$$

where

$$H(f) \triangleq \int_{-\infty}^{\infty} h(t)e^{-i2\pi ft}dt$$

is the transfer function for the filter. The input-output relation (31) is intuitively pleasing since the effect of filtering $x(t)$ is to scale the spectral component in $x(t)$ with frequency ν by the complex number $H(\nu)$. Thus, the individual spectral components that are averaged to form the SMF are each scaled by the appropriate value $H(f_j)$. It follows from (7) and (18) that the effects of filtering on the CTCF and the CP are given by

$$C_z^{\beta}(\boldsymbol{\tau})_n = \int_{-\infty}^{\infty} \cdots \int_{-\infty}^{\infty} \left[\prod_{j=1}^{n} h^{(*)_j}(\lambda_h)\right] C_x^{\beta}(\boldsymbol{\tau}-\boldsymbol{\lambda})_n d\boldsymbol{\lambda} \tag{32}$$

and

$$\bar{P}_z^{\beta}(\boldsymbol{f}')_n = \left[H^{(*)_n}((-)_n[\beta - \mathbf{1}^{\dagger}\boldsymbol{f}']) \prod_{j=1}^{n-1} H^{(*)_j}((-)_j f_j)\right] \times \bar{P}_x^{\beta}(\boldsymbol{f}')_n. \tag{33}$$

D. Periodic Time-Sampling

Let $z(t)$ be the product of an impulse train and the time-series $x(t)$

$$z(t) = y(t)x(t)$$
$$y(t) = \sum_{m=-\infty}^{\infty} \delta(t - mT_s)$$

where T_s is the sampling increment, and $f_s = 1/T_s$ is the sampling rate. Since $y(t)$ is periodic it is statistically independent of $x(t)$, and the results of Section IV–B can be used to find the nth-order parameters for $z(t)$.

The nth-order RD-CTMF for $z(t)$ is given by (cf. Section IV–B)

$$\bar{R}_z^{\alpha}(\boldsymbol{u})_n = \sum_{\gamma} \bar{R}_x^{\gamma}(\boldsymbol{u})_n \bar{R}_y^{\alpha-\gamma}(\boldsymbol{u})_n.$$

By using the formal identity

$$\sum_{m=-\infty}^{\infty} \delta(t - mT_s) = f_s \sum_{m=-\infty}^{\infty} e^{i2\pi mtf_s}$$

it is straightforward to show that the RD-CTMF for $y(t)$ is given by

$$\bar{R}_y^{\eta}(\boldsymbol{u})_n = f_s^n \sum_{\boldsymbol{m}} \left[\exp\{i2\pi f_s \boldsymbol{u}^{\dagger}\boldsymbol{m}'\}\kappa(\boldsymbol{m}^{\dagger}\mathbf{1}f_s - \eta)\right]$$

where

$$\boldsymbol{m} \triangleq [m_1 \cdots m_n]^{\dagger} \qquad \boldsymbol{m}' \triangleq [m_1 \cdots m_{n-1}]^{\dagger}$$

and

$$\kappa(x) = \begin{cases} 1, & x = 0 \\ 0, & x \neq 0 \end{cases}$$

is the Kronecker delta function. Thus, the RD-SMF for $z(t)$ is given by

$$\bar{S}_z^{\alpha}(\boldsymbol{f}')_n = f_s^n \sum_{\gamma} \left[\sum_{\boldsymbol{m}} \kappa(\boldsymbol{m}^{\dagger}\mathbf{1}f_s - \alpha + \gamma)\bar{S}_x^{\gamma}(\boldsymbol{f}' - \boldsymbol{m}'f_s)_n\right]. \tag{34}$$

Because $y(t)$ is periodic, the cumulant for $\{z(t+\tau_j)\}_{j=1}^n$ is given by (cf. Section IV–B)

$$C_z(t,\boldsymbol{\tau})_n = R_y(t,\boldsymbol{\tau})_n C_x(t,\boldsymbol{\tau})_n$$

and, therefore, the analysis above for the RD-SMF holds also for the RD-CTCF

$$\bar{C}_z^{\beta}(\boldsymbol{u})_n = \sum_{\eta} \bar{C}_x^{\eta}(\boldsymbol{u})_n \bar{R}_y^{\beta-\eta}(\boldsymbol{u})_n$$

and for the CP

$$\bar{P}_z^{\beta}(\boldsymbol{f}')_n = f_s^n \sum_{\gamma} \left[\sum_{\boldsymbol{m}} \kappa(\boldsymbol{m}^{\dagger}\mathbf{1}f_s - \beta + \gamma)\bar{P}_x^{\gamma}(\boldsymbol{f}' - \boldsymbol{m}'f_s)_n\right]. \tag{35}$$

The formulas (34) and (35) show that there are two kinds of aliasing effects due to sampling: (i) frequency aliasing, which is the overlapping of images of the CP (RD-SMF) with the same cycle frequency which occurs when $\gamma = \beta$ ($\gamma = \alpha$) in the sum and, (ii) cycle aliasing, which is the overlapping of images of the CP (RD-SMF) with cycle frequencies other than β (α).

V. Pulse-Amplitude Modulation

A. Cumulant Formulas for Complex PAM

In this section, we present the higher order parameters for complex-valued and, as a special case, real-valued pulse-amplitude-modulated (PAM) signals, which provide useful models for the classes of digital baseband and quadrature-amplitude-modulated (QAM) signals. The PAM time-series is given by

$$x(t) = \sum_{m=-\infty}^{\infty} a_m p(t + mT_0 + t_0) \tag{36}$$

where $\{a_m\}$ is an independent and identically distributed (IID) symbol sequence, $1/T_0$ is the symbol rate (or pulse rate), t_0 is an unknown constant that represents the absolute timing of the waveform, and $p(t)$ is the pulse function with Fourier transform given by $P(f)$

$$P(f) = \int_{-\infty}^{\infty} p(t)e^{-i2\pi ft}dt.$$

It is desired to calculate the CTCF and CP for $\{x^{(*)_j}(t+\tau_j)\}_{j=1}^n$.

The higher order cumulants for PAM time-series can be derived by using the results of Section IV, as sketched here The cumulants for arbitrary PAM signals can be derived from the cumulants for PAM signals that have rectangular pulses (or any other real-valued pulse shape with duration not exceeding

the reciprocal of the symbol rate). These latter cumulants can be shown [35] to be given by (for $t_0 = 0$)

$$C_x(t,\tau)_n = \text{Cumulant}\{x^{(*)_j}(t+\tau_j)\}_{j=1}^n = C_{a,n}\sum_{m=-\infty}^{\infty}\prod_{j=1}^{n} p(t+mT_0+\tau_j) \quad (37)$$

where $C_{a,n}$ is the nth-order cumulant of the symbol sequence, and is given by

$$C_{a,n} \triangleq \sum_{P_n}\left[(-1)^{p-1}(p-1)!\prod_{j=1}^{n} R_{a,\nu_j}\right]$$

in which

$$R_{a,\nu_j} \triangleq \lim_{K\to\infty}\frac{1}{2K+1}\sum_{k=-K}^{K}\prod_{q\in\nu_j} a_k^{(*)_q}. \quad (38)$$

The RD-CTCF and CP follow directly from (37):

$$\bar{C}_x^{\beta}(\boldsymbol{u})_n = \frac{C_{a,n}}{T_0}\int_{-\infty}^{\infty} p(t)\prod_{j=1}^{n-1} p(t+u_j)e^{-i2\pi\beta t}dt \quad (39)$$

$$\bar{P}_x^{\beta}(\boldsymbol{f}')_n = \frac{C_{a,n}}{T_0}P(\beta-\mathbf{1}^{\dagger}\boldsymbol{f}')\prod_{j=1}^{n-1}P(f_j) \quad (40)$$

where $\beta = k/T_0$.

An arbitrary PAM time-series (36) can be represented as a filtered impulse train $a(t)$:

$$x(t) = a(t)\otimes p(t+t_0)$$

where $\otimes$ represents the convolution operation, and $a(t)$ is a PAM signal of the type just analyzed, but with pulses equal to impulses. The cyclic cumulants and cyclic polyspectra for $x(t)$ can be determined by using the results in Section IV–C to determine the effect of filtering on these cyclic parameters.

The CP for $a(t)$ follows from (40) with $P(f) = 1$:

$$\bar{P}_a^{\beta}(\boldsymbol{f}')_n = \frac{C_{a,n}}{T_0}.$$

The effect of filtering the time-series $a(t)$ is easily determined by using (33) with the filter transfer function

$$H(f) = \int_{-\infty}^{\infty} p(t+t_0)e^{-i2\pi ft}dt = P(f)e^{i2\pi ft_0}.$$

Thus, the nth-order CP for $x(t)$ is given by

$$\bar{P}_x^{\beta}(\boldsymbol{f}')_n = \frac{C_{a,n}}{T_0}P^{(*)_n}((-)_n[\beta-\mathbf{1}^{\dagger}\boldsymbol{f}']) \times\prod_{j=1}^{n-1}P^{(*)_j}((-)_j f_j)e^{i2\pi\beta t_0} \quad (41)$$

which reduces to the following simpler form for real-valued time-series:

$$\bar{P}_x^{\beta}(\boldsymbol{f}')_n = \frac{C_{a,n}}{T_0}P(\beta-\mathbf{1}^{\dagger}\boldsymbol{f}')\prod_{j=1}^{n-1}P(f_j)e^{i2\pi\beta t_0}. \quad (42)$$

Inverse Fourier transforming (41) yields the RD-CTCF for PAM:

$$\bar{C}_x^{\beta}(\boldsymbol{u})_n = \frac{C_{a,n}}{T_0}\int_{-\infty}^{\infty} p^{(*)_n}(t) \times\prod_{j=1}^{n-1} p^{(*)_j}(t+u_j)e^{-i2\pi\beta t}dt\, e^{i2\pi\beta t_0}, \quad \beta = k/T_0. \quad (43)$$

B. Real-Valued Binary PAM

In the case of binary symmetric real PAM, the symbols take on the values ± 1 with equal FOT probability. For $n = 2$, the cumulant for the symbol variables is

$$C_{a,2} = 1.$$

Therefore, the second-order RD-CTCF is given by

$$\bar{C}_x^{\beta}(u)_2 = \frac{1}{T_0}\int_{-\infty}^{\infty} p(t)p(t+u)e^{-i2\pi\beta t}dt\, e^{i2\pi\beta t_0}, \quad \beta = k/T_0$$

and the second-order CP is given by

$$\bar{P}_x^{\beta}(f)_2 = \frac{1}{T_0}P(\beta-f)P(f)e^{i2\pi\beta t_0}$$

which for $\beta = 0$ reduces to the well-known formula for the PSD of a unity-power PAM signal

$$\bar{P}_x^{0}(f)_2 = \frac{1}{T_0}|P(f)|^2.$$

For $n = 4$, the cumulant for the symbol variables is given by

$$C_{a,4} = R_{a,4} - 3R_{a,2}^2 - 4R_{a,3}R_{a,1} + 12R_{a,2}R_{a,1}^2 - 6R_{a,1}^4 = R_{a,4} - 3R_{a,2}^2 = -2$$

where $R_{a,k}$ is given by

$$R_{a,k} \triangleq \lim_{K\to\infty}\frac{1}{2K+1}\sum_{m=-K}^{K} a_m^k.$$

Thus, the fourth-order RD-CTCF is given by

$$\bar{C}_x^{\beta}(\boldsymbol{u})_4 = \frac{-2}{T_0}\int_{-\infty}^{\infty} p(t)\prod_{j=1}^{3} p(t+u_j)e^{-i2\pi\beta t}dt\, e^{i2\pi\beta t_0}.$$

The magnitude of this function for $u_3 = 0$ is shown in Figs. 1 and 2 for $\beta = 0$ and $\beta = 1/T_0$ for two different pulse shapes. The pulse shape for Fig. 1 is rectangular:

$$p(t) = \begin{cases} 1, & |t| \le T_0/2 \\ 0, & \text{otherwise} \end{cases} \quad (44)$$

and the pulse shape for Fig. 2 is the inverse transform of the bandlimited pulse transform

$$P(f) = \begin{cases} 1, & |f| \le 1/2T_0 \\ 0, & |f| > 1/2T_0 \end{cases} \quad (45)$$

which is $\sin(\pi t/T_0)/\pi t$.

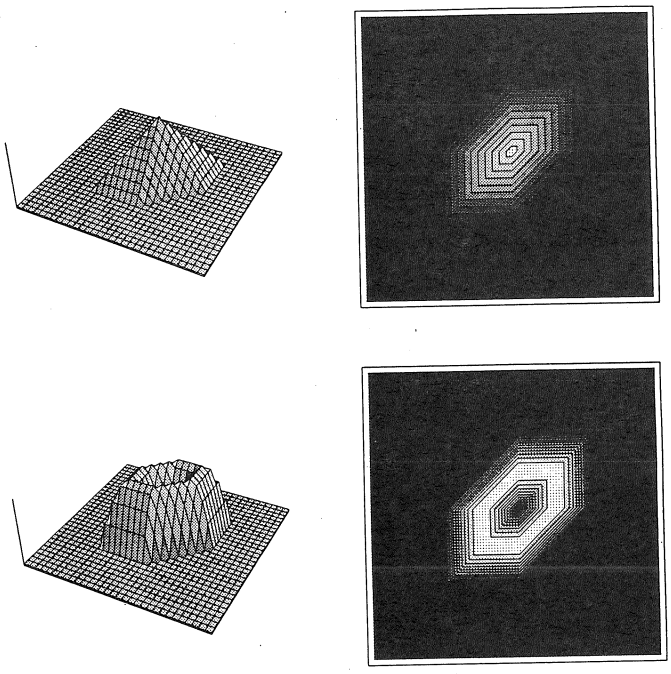

Fig. 1. Surface and contour plots for the magnitude of the ideal fourth-order RD-CTCF for binary PAM with full-duty-cycle rectangular pulses for $u_1, u_2 \in [-2T_0, 2T_0)$ and $u_3 = 0$. Upper plots correspond to $\beta = 0$, lower plots correspond to $\beta = 1/T_0$.

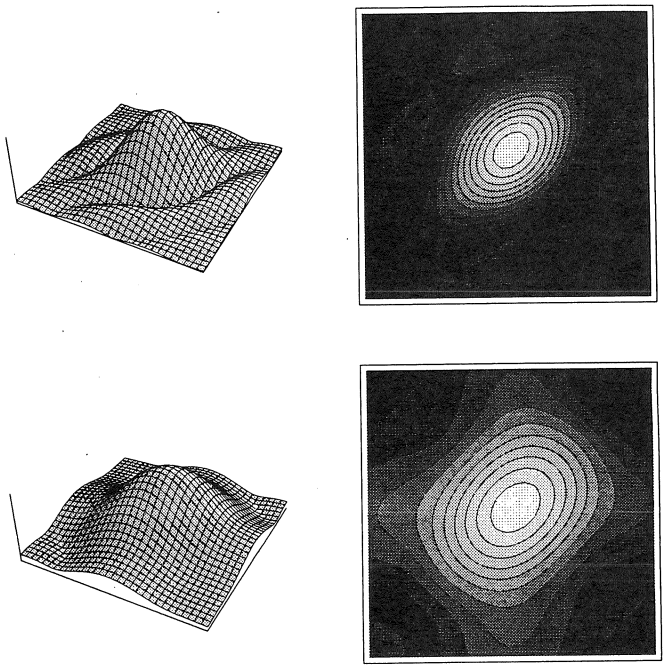

Fig. 2. Surface and contour plots for the magnitude of the ideal fourth-order RD-CTCF for binary PAM with zero-excess-bandwidth Nyquist pulses for $u_1, u_2 \in [-2T_0, 2T_0)$ and $u_3 = 0$. Upper plots correspond to $\beta = 0$, lower plots correspond to $\beta = 1/T_0$.

C. Complex-Valued Quaternary PAM

Consider the complex PAM signal (36) with symbol constellation $\{\pm 1, \pm i\}$ (equally probable), and a pulse with transform given by (45). This is a model for the complex envelope of a bandwidth-efficient quaternary-phase-shift-keyed (QPSK) signal. This signal has no second-order cyclostationarity because for $n = 2$ and the choice of no conjugations (or for two conjugations) $C_{a,2} = 0$, and for the choice of one conjugation, $C_{a,2} = 1$, but because of (45), the RD-CTCF is zero:

$$\int_{-\infty}^{\infty} p(t)p^*(t+u)e^{-i2\pi\beta t}dt = \int_{-\infty}^{\infty} P(f)P^*(f-\beta)e^{-i2\pi fu}df e^{i2\pi\beta u} = 0, \quad \beta = k/T_0, k \neq 0.$$

Nevertheless, this PAM signal exhibits fourth-order cyclostationarity for two choices of conjugations. In the first case, there are no conjugations and therefore

$$C_{a,4} = R_{a,4} - 3R_{a,2}^2 - 4R_{a,3}R_{a,1} + 12R_{a,2}R_{a,1}^2 - 6R_{a,1}^4 = R_{a,4} - 3R_{a,2}^2 = R_{a,4} = 1$$

which implies that

$$\bar{C}_x^{\beta}(\boldsymbol{u})_4 = \frac{1}{T_0}\int_{-\infty}^{\infty} p(t)\prod_{j=1}^{3} p(t+u_j)e^{-i2\pi\beta t}dt e^{i2\pi\beta t_0}, \quad \beta = k/T_0.$$

In the second case, two variables are conjugated, that is, the set of variables under consideration is

$$\{x(t+\tau_1)\; x(t+\tau_2)\; x^*(t+\tau_3)\; x^*(t+\tau_1)\}.$$

In this case, the cumulant for the symbol variables simplifies to $C_{a,4} = -1$, and the cumulant for the PAM time-series is given by

$$\bar{C}_x^{\beta}(\boldsymbol{u})_4 = \frac{-1}{T_0}\int_{-\infty}^{\infty} p^*(t)p(t+u_1)p(t+u_2) \times p^*(t+u_3)e^{-i2\pi\beta t}dt\, e^{i2\pi\beta t_0}, \quad \beta = k/T_0.$$

Note, however, that a different symbol distribution (e.g., uniform over the 8th roots of unity) could render $C_{a,4} = 0$ in both of the preceding cases, but some higher order cumulant (e.g., $n = 8$) would be nonzero.

VI. Measurement of HOCS Parameters

The measurement (estimation) of HOCS parameters from a single finite-length data record is considered in this section. This study is motivated by the need for such estimates that is demonstrated by the applications discussed in Section VII.

As explained in considerable detail in [11], the FOT-probability framework for the theory of cyclostationarity arises naturally when we conceptually start our inquiry with practical measurements and then idealize these measurements by letting measurement times approach infinity and, where relevant, letting spectral resolution bandwidths approach zero. These idealized measurements are the statistical parameters in terms of which the theory is formulated. These parameters include FOT probability densities, and the various temporal and spectral parameters of HOCS. Thus, it is quite obvious that the practical measurements can be interpreted as estimates of the idealized statistical parameters of the theory, which can be obtained only in the limit.

The measurement problem as formulated here may be somewhat confusing for the reader indoctrinated in statistical inference for stochastic processes because here the theoretical parameters to be measured are all mathematically defined in terms of a single infinite-length time-series, whereas the estimation problem formulated in the classical theory of statistical inference involves using a single finite-length data-record to estimate a theoretical parameter that is mathematically defined in terms of an associated stochastic process—an abstraction that cannot be derived by any form of idealization of actual measurement on a single time-series. Although the estimation methods described here can be viewed as the result of "backing off" from the limits that define the theoretical parameters, and then manipulating the resulting expressions to derive various estimators, they can alternatively be thought of in conjunction with a cycloergodic stochastic process (cf. Section I–C of Part I), in which case the measurements are interpreted as estimators of the parameters of this stochastic process.

Measurement of the polyspectrum for strictly stationary stochastic processes is considered in detail in [3], [30], [29], and [38], and to some extent estimation of the CP is similar. Because a natural first step (for the reader familiar with the HOS literature) in constructing estimators for HOCS parameters is to generalize this work on stationary processes to cyclostationary time-series, it is important to understand the estimation methods outlined in these references. This requires an understanding of the conditions under which the RD-SMF is equal to the CP because the methods of [3], [30], and [29] use estimates of the RD-SMF to estimate the polyspectrum. It should be emphasized that it is not desirable to estimate the RD-SMF over its entire domain of definition because it is generally impulsive, and can contain products of impulses. However, it is desired to estimate the simpler RD-SMF wherever it is equal to the CP, because it is the CP that we are interested in.

The conditions for equality between the RD-SMF and the CP can be determined by expressing the RD-CTMF in terms of the RD-CTCF and lower order CTMF's (cf. (9))

$$R_x^{\beta}(\boldsymbol{\tau})_n = C_x^{\beta}(\boldsymbol{\tau})_n - \sum_{\substack{P_n \\ p\neq 1}} \left[(-1)^{p-1}(p-1)! \times \sum_{\boldsymbol{\alpha}^{\dagger}\mathbf{1}=\beta} \prod_{j=1}^{p} R_x^{\alpha_j}(\boldsymbol{\tau}_{\nu_j})_{n_j} \right] \tag{46}$$

where $\boldsymbol{\tau} = [u_1 \cdots u_{n-1}\ 0]^{\dagger}$, and Fourier transforming in the u_j variables to obtain

$$\bar{S}_x^{\beta}(\boldsymbol{f}')_n = \bar{P}_x^{\beta}(\boldsymbol{f}')_n - \sum_{\substack{P_n \\ p\neq 1}} \left[k(p) \sum_{\boldsymbol{\alpha}^{\dagger}\mathbf{1}=\beta} \bar{S}_x^{\alpha_p}(\boldsymbol{f}'_{\nu_p})_{n_p} \times \prod_{j=1}^{p-1} \bar{S}_x^{\alpha_j}(\boldsymbol{f}'_{\nu_j})_{n_j} \delta(\boldsymbol{f}_{\nu_j}^{\dagger}\mathbf{1} - \alpha_j) \right] \tag{47}$$

where $k(p) = (-1)^{p-1}(p-1)!$, the $\boldsymbol{f}_{\nu_j}$ correspond to subsets of the the n-vector

$$\boldsymbol{f} = [f_1\ f_2 \cdots f_{n-1}\quad \beta - \mathbf{1}^{\dagger}\boldsymbol{f}'] \tag{48}$$

and $\boldsymbol{f}'_{\nu_j}$ is a vector of the first $n_j - 1$ elements of $\boldsymbol{f}_{\nu_j}$. To derive (47), it is assumed (without loss of generality) that each partition is ordered such that ν_p always contains n as its last element in (46), and (21) is used to transform each of the CTMF's in the products in the sum over P_n in (46), except for the one with reduced dimension (corresponding to the partition element ν_p), for which (17) is used.

It is clear that $\bar{S}_x^{\beta}(\boldsymbol{f}')_n$ is equal to $\bar{P}_x^{\beta}(\boldsymbol{f}')_n$ only if the sum over P_n in (47) is zero, which will happen if one or more of the impulse functions is zero for each partition. This will be the case for all $\boldsymbol{f}'$ except those that lie on a *β-submanifold*. The β-submanifolds are the sets of $\boldsymbol{f}'$ vectors for which there is at least one partition with $p > 1$ for which there is at least one $\boldsymbol{\alpha}$ in (47) such that the argument of each associated impulse function is zero, in which case that impulse is nonzero. Another way to express the β-submanifold set is: $\boldsymbol{f}'$ lies on a β-submanifold if the augmented vector (48) can be partitioned such that the sum of the f_j in each subset vector $\boldsymbol{f}_{\nu_k}$ corresponding to the partition element ν_k is an n_kth-order cycle frequency for $x(t)$ ($n_k = |\nu_k|$). This latter expression can be derived by forcing equality between the SMF and SCF. By examining (46) and (47), we see that moments and cumulants in both the time and frequency domains differ if there are lower order cycle frequencies, whose orders sum to n, that sum to the nth-order cycle frequency of interest. It is important to note that the function $\bar{S}_x^{\beta}(\boldsymbol{f}')_n$ is *not* impulsive at a value of $\boldsymbol{f}'$ that lies on a β-submanifold unless all the lower order coefficients $\bar{S}_x^{\alpha_j}(\boldsymbol{f}'_{\nu_j})_{n_j}$ of the impulses are themselves nonzero.

If $x(t)$ is strictly stationary, then the set of mth-order cycle frequencies is either the null set or $\{0\}$ for each m, and our condition for equality between the the RD-SMF and CP (for $\alpha = \beta = 0$) is that there does not exist any proper subset of the elements of the vector

$$\boldsymbol{f} = [f_1\ f_2 \cdots f_{n-1}\ -\mathbf{1}^{\dagger}\boldsymbol{f}']$$

such that the frequencies in this subset sum to zero, which is exactly the condition stated in [29] for the equality of the stochastic RD-SMF and polyspectrum for a strictly stationary stochastic process.

The method of estimating the polyspectrum for strictly stationary processes that is proposed in [3] and [29] is based on the *higher order periodogram* defined by

$$I_{x_T}^0(t, \boldsymbol{f}')_n \triangleq \frac{1}{T} X_T^{(*)_n}(t, -\mathbf{1}^{\dagger}\boldsymbol{f}') \prod_{j=1}^{n-1} X_T^{(*)_j}(t, f_j).$$

The idea is to smooth this function over the $n-1$ variables $\boldsymbol{f}'$ with an $(n-1)$-dimensional window $W(\boldsymbol{f}')$ *while avoiding the inclusion of values of $I_{x_T}^0(t, \boldsymbol{f}')_n$ for $\boldsymbol{f}'$ that lie on a 0-submanifold*. It is shown in [29] that this method is asymptotically unbiased and consistent provided that the window function, which depends on the data-length T and on n, satisfies certain conditions related to its rate of decay. This frequency-smoothing method is also presented in Priestley's book [30]. However, Priestley does not force the smoothing window to be zero on the 0-submanifolds. His single example of the method uses a zero-mean time-series and $n = 3$, in which case there are no 0-submanifolds to avoid.

In [2], [3], and [29], the measurement parameter T is coupled with the width of the window $W(\boldsymbol{f}')$. In the approaches for estimating the CP discussed in this paper, the width of the spectral smoothing window is a parameter that is decoupled from the data-length parameter T. That is, in the methods for estimating the frequency-domain parameters of the RD-SMF and CP, two independent measurement parameters are explicitly used: the frequency-smoothing window width Δf and the data length T. This is consistent with the theory of second-order cyclostationarity in [11], and is appropriate because in actual measurement situations, the operator should be able to choose T and Δf independently.

Before generalizing the frequency-smoothing technique to the case of the cyclic polyspectrum, we first consider measurement of the time-domain moments and cumulants. Then we present several estimators of the CP. All measurement methods considered here, except for the frequency-smoothing technique, were obtained by generalizing from order $n = 2$ to $n > 2$ and from moments to cumulants the methods proposed in [11]. The frequency-smoothing method could also have been obtained by generalizing the corresponding method from [11] but, in fact, was obtained by generalizing the method of [2] and [3].

A. Time-Domain Parameters

We are given the finite-length portion $x(u) : u \in [t - T/2, t + T/2]$ of a persistent time-series. This portion has length T and center t, and can be expressed as

$$x(u)\ \text{rect}\left[\frac{u-t}{T}\right]$$

where

$$\text{rect}(t) \triangleq \begin{cases} 1, & |t| \le 1/2 \\ 0, & |t| > 1/2. \end{cases}$$

The nth-order lag product for this segment is given by

$$L_{x_T}(u,t,\boldsymbol{\tau})_n = \prod_{j=1}^{n} x(u+\tau_j)\text{rect}\left[\frac{u+\tau_j-t}{T}\right].$$

The estimator for the CTMF $R_x^{\alpha}(\boldsymbol{\tau})_n$ is

$$R_{x_T}^{\alpha}(t,\boldsymbol{\tau})_n \triangleq \frac{1}{T}\int_{-\infty}^{\infty} L_{x_T}(u,t,\boldsymbol{\tau})_n e^{-i2\pi\alpha u}du.$$

which can be expressed as

$$R_{x_T}^{\alpha}(t,\boldsymbol{\tau})_n \triangleq \frac{1}{T}\int_{t_l}^{t_u}\prod_{j=1}^{n} x^{(*)_j}(v+\tau_j)e^{-i2\pi\alpha v}dv \qquad (49)$$

where $t_l = t - T/2 - \min\{\tau_j\}$, $t_u = t + T/2 - \max\{\tau_j\}$, and $t_u \ge t_l$. If $t_u < t_l$, the estimate is defined to be zero because in this case the delays are so widely separated that the shifted data segments do not overlap. The estimate (49) converges to the theoretical CTMF

$$\lim_{T\to\infty} R_{x_T}^{\alpha}(t,\boldsymbol{\tau})_n = R_x^{\alpha}(\boldsymbol{\tau})_n$$

since $R_x^{\alpha}(\boldsymbol{\tau})_n$ is *defined* to be the pointwise limit of $R_{x_T}^{\alpha}(t,\boldsymbol{\tau})_n$.

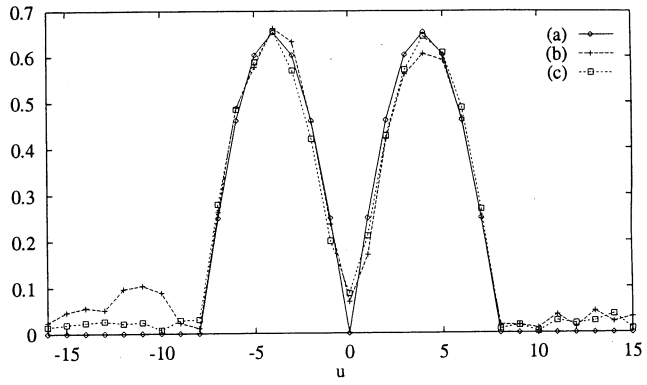

Fig. 3. Fourth-order RD-CTCF's for binary PAM with full-duty-cycle rectangular pulses for $\boldsymbol{u} = [0\ 0\ u]$, $\beta = 1/T_0$, and SNR = 0 dB: (a) Theory; (b) $T = 512T_0$; (c) $T = 2048T_0$ ($T_0 = 8$).

The estimator for the CTCF is given by the combination of lower order CTMF estimates specified by (8):

$$C_{x_T}^{\beta}(t,\boldsymbol{\tau})_n \triangleq \sum_{P_n}\left[(-1)^{p-1}(p-1)!\times\sum_{\boldsymbol{\alpha}^{\dagger}\mathbf{1}=\beta}\prod_{j=1}^{p}R_{x_T}^{\alpha_j}(t,\boldsymbol{\tau}_{\nu_j})_{n_j}\right] \qquad (50)$$

where the second sum is over all vectors $\boldsymbol{\alpha} = [\alpha_1 \cdots \alpha_p]^{\dagger}$ of cycle frequencies with orders $n_1 \cdots n_p$ that sum to β: $\boldsymbol{\alpha}^{\dagger}\mathbf{1} = \beta$. Since each CTMF estimate converges to its theoretical parameter, we have the following convergence (assuming that the possibly infinite but denumerable sum over $\boldsymbol{\alpha}$ can be interchanged with the limit)

$$\lim_{T\to\infty} C_{x_T}^{\beta}(t,\boldsymbol{\tau})_n = C_x^{\beta}(\boldsymbol{\tau})_n.$$

In order to construct the estimate (50), all lower order cycle frequencies for $x(t)$ must be known or estimated; an algorithm for estimating these frequencies is described in Section VII. To estimate the RD-CTMF and RD-CTCF, we set $\boldsymbol{\tau} = [u_1 \cdots u_{n-1}\ 0]$ in (49) and (50), respectively.

The mean and variance of the estimator (49), derived in [35], are given in Appendix B.

1) Examples: Consider the PAM signal (36) with full-duty-cycle rectangular pulses (44), $T_0 = 8$, and a sequence of binary (± 1) symbols that occur with equal probability. A portion of the theoretical fourth-order RD-CTCF for this signal is shown in Fig. 1. To verify the correctness of the estimators of the CTMF and CTCF, we simulate this signal and use discrete-time versions of the estimators (49) and (50) to obtain estimates. Fig. 3 shows the theoretical and measured fourth-order RD-CTCF for $\beta = 1/T_0$ for the PAM signal described above in white Gaussian noise (WGN) such that the signal and noise have equal power. These RD-CTCF's were estimated using the second-order cycle frequencies k/T_0 for $|k| \le 3$. Contributions from cycle frequencies k/T_0 for $|k| > 3$ were found to be negligible. A reasonable estimate is obtained for an observation interval length T of 512 symbols, and a good estimate is obtained for $T = 2048$ symbols.

Fig. 4 shows the same measurements for a binary PAM signal with Nyquist pulses that have 0% excess bandwidth

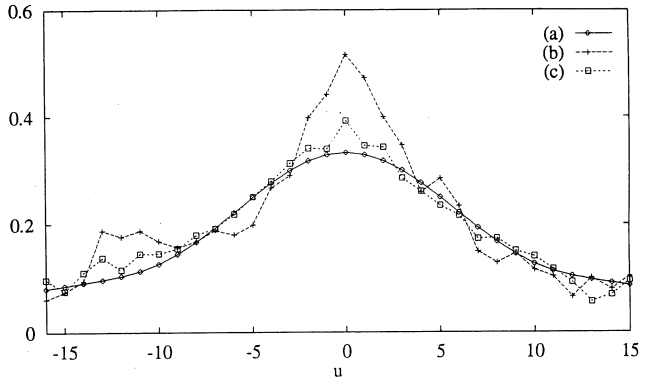

Fig. 4. Fourth-order RD-CTCF's for binary PAM with Nyquist pulses having zero excess bandwidth for $\boldsymbol{u} = [0\ 0\ u]$, $\beta = 1/T_0$, and SNR = 0 dB: (a) Theory; (b) $T = 1024T_0$; (c) $T = 4096T_0$ ($T_0 = 8$).

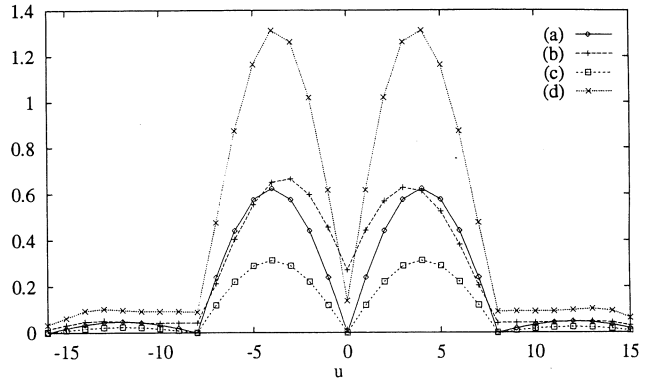

Fig. 5. Fourth-order RD-CTCF and RD-CTMF estimates for the sum of two equipower PAM signals ($x = s_1 + s_2$) with full-duty-cycle rectangular pulses having symbol rates β_1 and β_2, for cycle frequency β_1, $\boldsymbol{u} = [0\ 0\ u]$, and $T = 2048T_0$: (a) RD-CTCF for $s_1(t)$; (b) RD-CTCF for $x(t)$; (c) RD-CTMF for $s_1(t)$; (d) RD-CTMF for $x(t)$ ($\beta_1 = 1/T_0 = 1/8, \beta_2 = 1/5$).

(45). A portion of the theoretical fourth-order RD-CTCF for this signal is shown in Fig. 2. The only lower order cycle frequency for this signal is $\alpha = 0$ for $n = 2$. A much larger value of T is required to obtain a reasonable estimate for this signal.

Finally, Fig. 5 shows the fourth-order RD-CTMF and RD-CTCF for the sum of two equipower full-duty-cycle rectangular-pulse PAM signals with distinct symbol interval lengths of 8 and 5. The cycle frequency is $\beta = 1/8$, and the lower order cycle frequencies are those corresponding to the first signal, $k/8$ for $|k| \leq 3$ for $n = 2$, because these are the only lower order cycle frequencies that can add to the cycle frequency of the measurement, $1/8$. This figure shows that the RD-CTCF is signal selective, whereas the RD-CTMF is not. That is, if the symbol rate is known, the measured RD-CTCF asymptotically approaches the theoretical RD-CTCF for the signal of interest, but the measured RD-CTMF does not approach the theoretical RD-CTMF for the signal of interest. This confirms the theory regarding signal selectivity given in Section IV.

B. Estimating the Cyclic Polyspectrum

As explained in [35], the CP can be estimated by Fourier transforming a windowed estimate of the RD-CTCF:

$$\bar{P}^{\beta}_{x_T}(t, \boldsymbol{f}')_{\Delta f} = \int_{-\infty}^{\infty} \cdots \int_{-\infty}^{\infty} w_{1/\Delta f}(\boldsymbol{u}) \times \bar{C}^{\beta}_{x_T}(t, \boldsymbol{u})_n e^{-i2\pi \boldsymbol{u}^{\dagger} \boldsymbol{f}'} d\boldsymbol{u}, \quad (51)$$

$$w_{1/\Delta f}(\boldsymbol{u}) = \prod_{j=1}^{n-1} \text{rect}(u_j \Delta f).$$

The multidimensional window $w_{1/\Delta f}(\boldsymbol{u})$ can be replaced by any function with finite support in $(n-1)$-dimensional Euclidean space such that its Fourier transform converges (formally) to a product of Dirac delta functions:

$$\lim_{\Delta f \to 0} \mathcal{F}^{n-1}\{w_{1/\Delta f}(\boldsymbol{u})\} = \prod_{j=1}^{n-1} \delta(f_j).$$

The CP can also be estimated by first constructing the *nth-order cyclic periodogram*

$$I^{\beta}_{x_T}(t, \boldsymbol{f}')_n \triangleq \frac{1}{T} X^{(*)n}_T(t, (-)_n[\beta - \mathbf{1}^{\dagger}\boldsymbol{f}']) \prod_{j=1}^{n-1} X^{(*)_j}_T(t, (-)_j f_j) = \mathcal{F}^{n-1}\{\bar{R}^{\beta}_{x_T}(t, \boldsymbol{u})_n\} \quad (52)$$

masking it by a special function $Z_{\beta}(\boldsymbol{f}')$, and then convolving with a multidimensional smoothing window [31], [32], [19], [7], [35]:

$$\bar{P}^{\beta}_{x_T}(t, \boldsymbol{f})_{\Delta f} = W_{\Delta f}(\boldsymbol{f}') \otimes \left[I^{\beta}_{x_T}(t, \boldsymbol{f}')_n Z_{\beta}(\boldsymbol{f}')\right]. \quad (53)$$

In (53), $Z^{\beta}(\boldsymbol{f}')$ is equal to one except at those $\boldsymbol{f}'$ that lie on β-submanifolds, in which case it is equal to zero. The vector $[g_1 \cdots g_n]$, for $g_n = \beta - \sum_{j=1}^{n-1} g_j$, lies on a β-submanifold if there is at least one partition $\{\nu_j\}_{j=1}^{p}$ in P_n with $p > 1$ such that each sum $\alpha_k = \sum_{k \in \nu_j} g_k$ is an n_jth-order cycle frequency of $x(t)$ (for the set of optional conjugations that are chosen). As mentioned previously, these β-submanifolds must be avoided in the convolution (53) because the smoothed nth-order cyclic periodogram converges to the function $\bar{S}^{\beta}_x(\boldsymbol{f}')_n$, which can contain multiple impulsive factors for values of $\boldsymbol{f}'$ that lie on β-submanifolds, but which, for all other $\boldsymbol{f}'$, is equal to the nonimpulsive function $\bar{P}^{\beta}_x(\boldsymbol{f}')_n$. These impulses are avoided in the method (51) because the additive sine-wave components in the $\boldsymbol{u}$ variables of the RD-CTMF estimate $\bar{R}^{\beta}_x(t, \boldsymbol{u})_n$ are removed in forming the RD-CTCF estimate $\bar{C}^{\beta}_{x_T}(t, \boldsymbol{u})_n$, and it is these additive sine waves that give rise to the (smoothed) spectral lines in the transform $I^{\beta}_{x_T}(t, \boldsymbol{f}')_n$ of $\bar{R}^{\beta}_{x_T}(t, \boldsymbol{u})_n$. This transform relation (52) is a generalization of the cyclic periodogram-correlogram relation introduced in [11] from $n = 2$ to all n.

There are several difficulties associated with this frequency-smoothing method. The first is that although the impulsive parts of the RD-SMF are avoided by the smoothing operation, there can be substantial leakage from the impulses into nearby regions in $\boldsymbol{f}'$, which are exactly the regions used to compute the CP estimate for $\boldsymbol{f}'$ that are on the β-submanifolds. This can be seen by considering the simple case of $n = 2$. If the data contains additive finite-strength sine wave components, then the spectrum contains impulses. To estimate the continuous portion of the spectrum at a point where there is an impulse due to the discrete portion of the spectrum is problematic when

using frequency smoothing because of leakage. This leakage problem is discussed further and is illustrated with numerical examples in Section VI–B–2. This leakage problem, which is common knowledge for $n = 2$, is not mentioned in [2], [3], or [30] for the case of stationary stochastic processes, nor in [19] or [7] for the case of cyclostationary stochastic processes. In addition to the leakage problem, the frequency-smoothed cyclic periodogram method is computationally costlier than the Fourier transformed RD-CTCF method (51) for $n > 2$, even when there are no β-submanifolds to avoid [35] This is surprising since the opposite is known to be true for $n = 2$.

Finally, the CP can be estimated for values of $\boldsymbol{f}'$ that do not lie on β-submanifolds by time-averaging the masked higher order cyclic periodogram

$$\bar{P}^{\beta}_{x_T}(t, \boldsymbol{f}')_{1/\Delta f} = g_T(t) \otimes \left[I^{\beta}_{x_{1/\Delta f}}(t, \boldsymbol{f}')_n Z_{\beta}(\boldsymbol{f}') \right] \quad (54)$$

where

$$g_T(t) = \begin{cases} 1/T, & |t| \le T/2 \\ 0, & \text{otherwise.} \end{cases}$$

Unlike the frequency-smoothing method, the time-averaging method cannot produce estimates of the CP for frequencies $\boldsymbol{f}'$ that lie on β-submanifolds without modification. An example of such a modification to (54) is to compute estimates of the CP for values of $\boldsymbol{f}'$ that are near to the β-submanifolds, and then use interpolation to estimate the value of the CP for the $\boldsymbol{f}'$ that are on the β-submanifolds.

The three methods of estimating the CP converge to the theoretical CP [35] in the sense that

$$\begin{aligned} \bar{P}^{\beta}_{x}(\boldsymbol{f}')_n &= \lim_{\Delta f \to 0} \lim_{T \to \infty} \bar{P}^{\beta}_{x_T}(t, \boldsymbol{f}')_{\Delta f} \\ &= \lim_{\Delta f \to 0} \lim_{T \to \infty} \bar{P}^{\beta}_{x_T}(t, \boldsymbol{f}')_{1/\Delta f}. \end{aligned} \quad (55)$$

It is worth pointing out that the three estimators of the CP presented in this section each reduce to a well-known estimator of the PSD for the case of $n = 2$ and zero-mean stationary signals. Specifically, (51) reduces to the Blackman-Tukey method (Fourier transformation of a tapered autocorrelation estimate), (53) reduces to the Wiener-Daniell method (frequency smoothing of the periodogram), and (54) reduces to the Bartlett-Welch method (time-averaging of the periodogram) ([11], Chapter 6). Similarly, each of the estimators of the CP can be considered as a generalization of estimators of the cyclic spectrum from second-order to higher orders ([11], Chapter 13). Finally, the estimators (51) and (53) are generalizations of estimators of the polyspectrum that were proposed by Brillinger and Rosenblatt [1]–[3], [29] from stationary stochastic processes to cyclostationary time-series.

1) Examples: The fourth-order CP is estimated by the time-averaging method (54) for the same signals and noises used to obtain the estimates of the RD-CTCF and RD-CTMF in Figs. 3–5.

The theoretical and measured fourth-order cyclic polyspectra for the case of binary PAM with full-duty-cycle rectangular pulses in WGN for $\beta = 1/T_0$ are shown in Fig. 6. The data segment length used to form the fourth-order cyclic periodogram is 64, which results in a frequency resolution

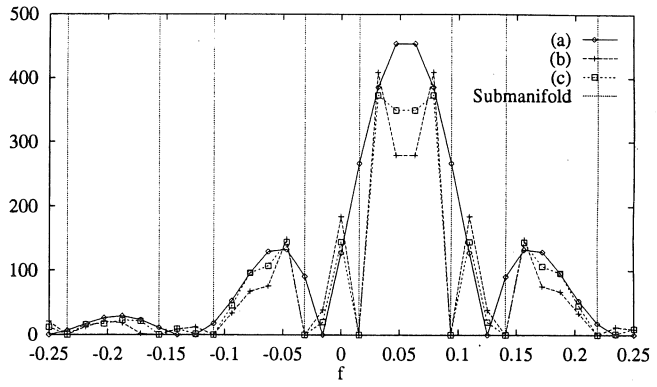

Fig. 6. The fourth-order CP from (54) for binary PAM with full-duty-cycle rectangular pulses, $\boldsymbol{f}' = [1/32\ 1/64\ f]$, $\beta = 1/T_0$, $\Delta f = 1/8T_0$, and SNR = 0 dB: (a) Theory, (b) $T = 512T_0$, (c) $T = 2048T_0$ ($T_0 = 8$).

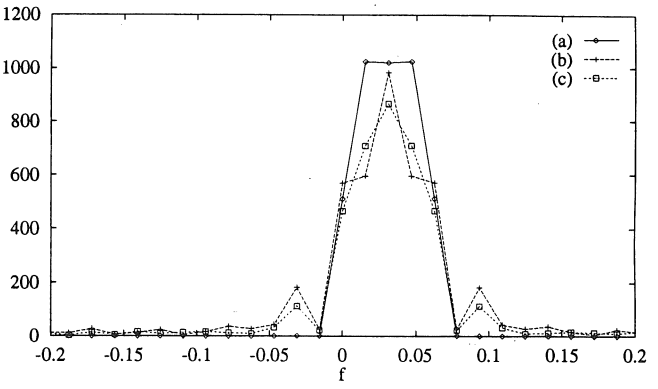

Fig. 7. The fourth-order CP from (54) for binary PAM with Nyquis pulses having zero excess bandwidth, $\boldsymbol{f}' = [1/32\ 1/32\ f]$, $\beta = 1/T_0$, $\Delta f = 1/8T_0$, and SNR = 0 dB. (a) Theory, (b) $T = 512T_0$, (c) $T = 4096T_0$ ($T_0 = 8$).

of Δf =1/64. The lower order cycle frequencies used to compute the β-submanifold points are $k/T_0 = k/8$ for $|k| \le 3$ for $n = 2$; cycle frequencies equal to higher harmonics of the symbol rate ($|k| > 3$) can be neglected because they correspond to cyclic features that are relatively small. There are eight β-submanifold points in the specified domain of the estimate; these points are marked on the graph. The output of the estimator is defined (arbitrarily) to be zero at these points. Note that linear interpolation would yield good estimates of the CP for the β-submanifold points in the main lobe in Fig. 6.

The theoretical and measured fourth-order cyclic polyspectra for the case of binary PAM with Nyquist pulses having 0% excess bandwidth are shown in Fig. 7 (cf. Figs. 2 and 4). The measurement parameters are the same as in the previous case, except that there is only one lower order cycle frequency: $\alpha = 0$ for $n = 2$. Thus, there are no β-submanifolds for $\beta = 1/T_0 = 1/8$.

Finally, the CP for the case of the sum of two equipower PAM signals with full-duty-cycle rectangular pulses, having distinct symbol rates $1/8$ and $1/5$ for $\beta = 1/8$ is shown in Fig. 8 (cf. Fig. 5). The lower order cycle frequencies used to compute the β-submanifold points are $k/8$ for $|k| \le 3$ fc $n = 2$.

2) Leakage from β-Submanifolds: A leakage effect exists in the method (53) that is due to the smearing of the im-

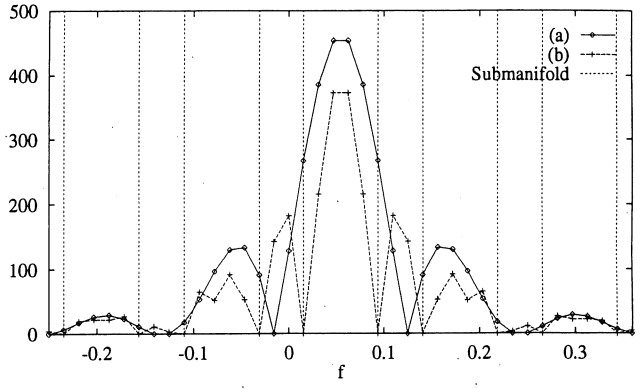

Fig. 8. Fourth-order CP from (54) for the sum of two equipower PAM signals ($x = s_1 + s_2$) with full-duty-cycle rectangular pulses, having symbol rates β_1 and β_2 for cycle frequency β_1, $\boldsymbol{f}' = [1/32\ 1/64\ f]$, $\Delta f = 1/8T_0$: (a) Theory for $s_1(t)$; (b) CP estimate for $x(t)$ for $T = 2048T_0$ ($T_0 = 1/\beta_1 = 8, \beta_2 = 1/5$).

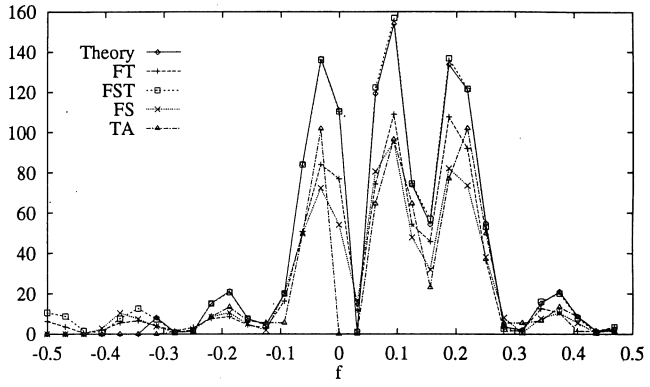

Fig. 9. Estimates of the fourth-order CP for binary PAM with full-duty-cycle rectangular pulses for $\beta = 1/T_0$, a collect time of $292T_0$, and $\boldsymbol{f}' \in S_1$. The TA estimate is defined to be zero at the two submanifold points $f = 0, 1/32$.

pulses on the β-submanifolds to neighboring regions off the β-submanifolds [32]. To quantify this leakage effect, the temporal mean of (53) is computed. From Appendix B

$$\langle \bar{R}_x^{\beta}(\boldsymbol{u})_n \rangle = \bar{R}_x^{\beta}(\boldsymbol{u})_n v_T(\boldsymbol{u})$$

where

$$v_T(\boldsymbol{u}) \triangleq \begin{cases} 1 + u_0(\boldsymbol{u})/T, & |u_0(\boldsymbol{u})| \le T \\ 0, & \text{otherwise} \end{cases}$$

and

$$u_0(\boldsymbol{u}) \triangleq \min\{0, u_1, \ldots, u_{n-1}\} - \max\{0, u_1, \ldots, u_{n-1}\}.$$

Using this result, it is easy to show that the temporal mean of (53) is given by the convolution

$$W_{\Delta f}(\boldsymbol{f}') \otimes \left[\left(\bar{S}_x^{\beta}(\boldsymbol{f}')_n \otimes V_T(\boldsymbol{f}') \right) Z_{\beta}(\boldsymbol{f}') \right]$$

where $V_T(\boldsymbol{f}')$ is the $(n-1)$-dimensional Fourier transform of $v_T(\boldsymbol{u})$. The effect of the convolution with $V_T(\boldsymbol{f}')$ is to smear the impulses in $\bar{S}_x^{\beta}(\boldsymbol{f}')_n$, thus producing spectral leakage into nearby regions, which cannot be removed by the masking function $Z_{\beta}(\boldsymbol{f}')$.

The method (51) also exhibits leakage when the CTMF's (6) are computed using an FFT algorithm, and the cycle frequencies α_j are not "on bin center." This leakage can be substantially reduced by computing each CTMF by evaluating the FST (the Fourier series transform, which is like the DFT but can be evaluated at an arbitrary value of frequency) for every α_j appearing in the sum in (50), but this can greatly increase the computational cost of the method [32], [35].

In the following, several fourth-order CP measurements are displayed graphically for the purpose of illustrating the relative performances of the CP estimators (51), (53), and (54) in the presence of leakage from the β-submanifolds.

The signal of interest is a binary pulse-amplitude-modulated signal with symbol interval length $T_0 = 7T_s$ and IID symbols. Both rectangular keying pulses rect(t/T_0) and Nyquist-shaped pulses are simulated. As before, only the second-order cycle frequencies k/T_0 for $|k| \le 3$ are used to compute the lower order CTMF's and to find the β-submanifolds for the case of rectangular pulses because the higher harmonics ($|k| > 3$) produce relatively weak features and can therefore be neglected. For Nyquist pulses, the only lower order cycle frequency is $\alpha = 0$ for $n = 2$.

The fourth-order CP for $\beta = 0$ and $\beta = 1/T_0$ is estimated for the observation interval length of 2048 ($\approx 292T_0$) samples using the following methods:

- FS: frequency-smoothing method (53)
- FT: Fourier-transformed RD-CTCF method (51) using FFT's to estimate the lower order CTMF's
- FST: Fourier-transformed RD-CTCF (51) using the FST for estimating the lower order CTMF's
- TA: time-averaging method (54).

For the time-domain methods (FT and FST), the RD-CTCF is estimated on the cubic grid of integers $\boldsymbol{u} = [u_1\ u_2\ u_3] \in [-8, 7]^3$, and then Fourier transformed. In the FS method, the spectral smoothing window width is set equal to 128 samples, and in the TA method, the block size is 32 samples. Thus, each method uses approximately the same temporal and spectral resolution parameters and can therefore be compared fairly.

Because computing the entire CP using (53) is relatively costly, and is difficult to display, only two "slices" of the CP were estimated. The slices correspond to $S_1 = [0.0\ 1/32\ f]$ for the case of rectangular pulses, and $S_2 = [1/32\ 1/32\ f]$ for the case of Nyquist pulse for $f \in \{k/32, k = -16, \ldots, 15\}$.

The CP estimates for ten independent realizations (with the same timing parameter t_0 in (36)) of the signals were averaged to produce the final set of estimates. The magnitudes of the estimates are shown in Figs. 9–12. Generally speaking, the FST method delivers the best performance because it suffers the least from the aforementioned leakage effect. However, it is not the best method from the point of view of computational cost [35].

C. Cycloergodicity and Measurement of Cumulants

We illustrate here the kind of error that can result from modeling a signal as a stationary stochastic process (or stationary time-series) when the sample paths are actually cyclostationary

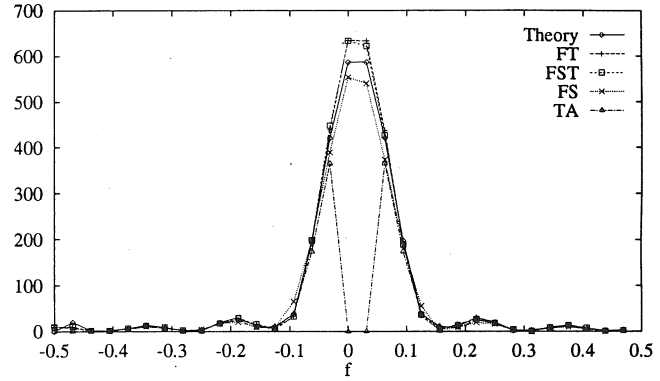

Fig. 10. Estimates of the fourth-order CP for binary PAM with full-duty-cycle rectangular pulses for $\beta = 0$, a collect time of $292T_0$, and $\boldsymbol{f}' \in S_1$. The TA estimate is defined to be zero at the two submanifold points $f = 0, 1/32$.

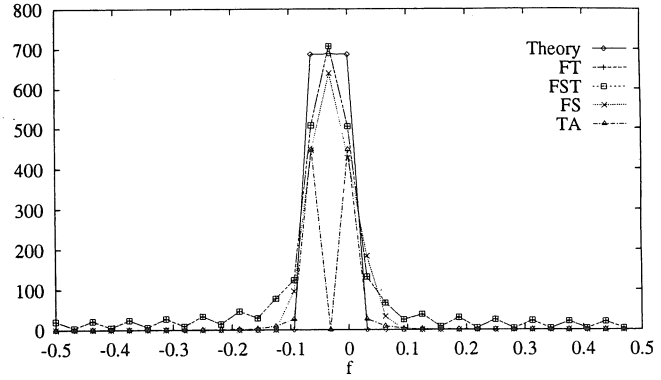

Fig. 12. Estimates of the fourth-order CP for binary PAM with Nyquist pulses having zero excess bandwidth for $\beta = 0$, a collect time of $292T_0$, and $\boldsymbol{f}' \in S_2$. The TA estimate is defined to be zero at the submanifold point $f = -1/32$.

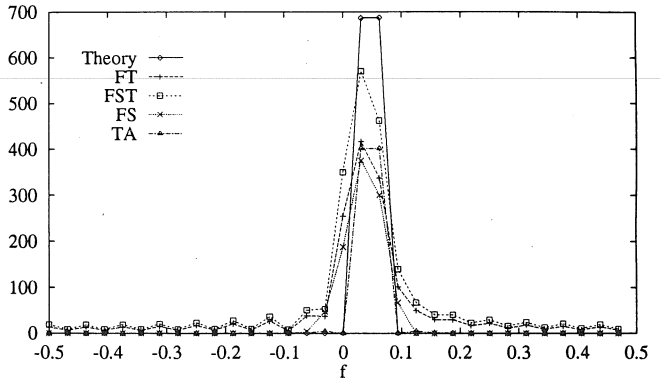

Fig. 11. Estimates of the fourth-order CP for binary PAM with Nyquist pulses having zero excess bandwidth for $\beta = 1/T_0$, a collect time of $292T_0$, and $\boldsymbol{f}' \in S_2$.

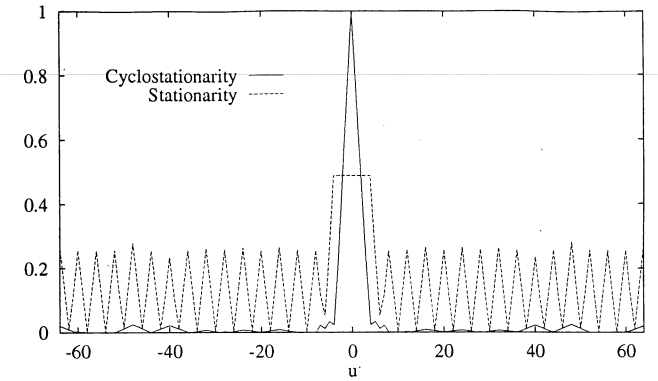

Fig. 13. Estimates of the fourth-order RD-CTCF for a binary PAM signal under the assumptions of stationarity and cyclostationarity.

time-series, and then measuring higher order parameters from a single sample path. Specifically, we consider a zero-mean, noiseless binary PAM signal with full-duty-cycle rectangular pulses, $\beta = 0$, $T = 512T_0$, and $n = 4$. If we think of the signal as stationary (e.g., by making the pulse timing parameter t_0 random and uniformly distributed over $[0, T_0]$ in the stochastic process model, we obtain a stationary process [9]) and compute the theoretical RD-CTCF we obtain

$$\bar{C}_x^0(\boldsymbol{u})_4 = \sum_{P_n} \left[(-1)^{p-1}(p-1)! \prod_{j=1}^{p} R_x^0(\boldsymbol{\tau}_{\nu_j})_{n_j} \right] \qquad (56)$$
$$\tau_i = u_i, \tau_4 = 0.$$

Hence, we are explicitly assuming that there are no lower order sine waves associated with $x(t)$ by modeling $x(t)$ as stationary and ignoring the lack of cycloergodicity in this model (cf. [39]). A portion of an estimate corresponding to this cumulant formula is represented by a dotted line in Fig. 13. The oscillatory portion of the estimate does not die out for large u. This oscillation is due to the interaction of second-order sine waves that have not been subtracted out of the fourth-order moment term in (56). On the other hand, if we recognize the cyclostationarity of the sample path and, therefore, take into account the second-order sine waves, we obtain the RD-CTCF

$$\bar{C}_x^0(\boldsymbol{u})_4 = \sum_{P_n} \left[(-1)^{p-1}(p-1)! \sum_{\boldsymbol{\alpha}^\dagger \mathbf{1}=0} \prod_{j=1}^{p} R_x^{\alpha_j}(\boldsymbol{\tau}_{\nu_j})_{n_j} \right] \qquad (57)$$
$$\tau_i = u_i, \tau_4 = 0.$$

A portion of an estimate corresponding to this cumulant formula is represented by the solid line in Fig. 13. Note that both graphs are estimates obtained from the same data record. The CP estimates that correspond to the two different assumptions are shown in Fig. 14. The size of the peak in the curve obtained by assuming stationarity grows with collect length T because this peak is due to the oscillatory portion of the RD-CTCF estimate, which does not die out with increasing $\boldsymbol{u}$.

Note that this phenomenon is usually not observed in the case of $n = 2$ because we typically consider zero-mean signals that do not contain finite-strength additive sine wave components. Thus, the PSD estimates agree with the calculated formula based on a stationary model, even when the signal is cyclostationary, because there are no lower order sine waves to deal with. This example suggests that the theory of HOCS is useful even in the case where cyclostationarity is of no interest but is exhibited by the data because if cyclostationarity is ignored, theory and practice will not agree.

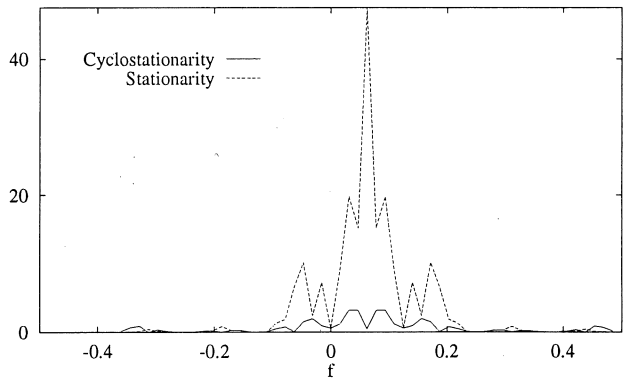

Fig. 14. Estimates of the fourth-order CP for a binary PAM signal under the assumptions of stationarity and cyclostationarity.

VII. Applications of HOCS

In general, the applications of the theory of HOCS are similar to those for the theory of SOCS and the theory of HOS, namely weak-signal detection, signal parameter estimation, system identification and equalization, and array-based direction-finding and blind adaptive spatial filtering. The use of cyclic cumulants or cyclic polyspectra rather than conventional cumulants or polyspectra can be advantageous when the corrupting signals are not Gaussian (manmade signals are rarely Gaussian), and the use of higher order cyclic parameters rather than second-order cyclic parameters can be advantageous when the signal does not exhibit second-order cyclostationarity, or when there are no cycle frequencies unique to the signal of interest for order two, but there are unique cycle frequencies for a higher order.

HOS-based detection algorithms are given in [18] and [24], and HOS-based time-delay estimation algorithms are given in [4], [22], and [37], where the signals are modeled as exponentially distributed stationary processes, and order three is focused upon. HOCS-based detection and time-delay estimation algorithms are given in [33], [7], and [20]. The methods given in [7] and [20] are distinct from those given in this section; the former attempt to exploit the asymptotic statistical nature of estimates of third-order cyclic cumulants, whereas the latter attempt to exploit the structure of arbitrary-order cyclic moments and cumulants. HOCS-based direction-finding methods (array based) are given in [21].

A. Weak-Signal Detection

In this section, we consider the problem of detecting the presence of a desired signal (or signals) $s(t)$ in a received data set $x(t)$ with noise and interference $n(t)$,

$$x(t) = s(t) + n(t), \qquad -T/2 \le t \le T/2.$$

There are several versions of the detection problem that are of interest. The first is called the *general search problem*, in which we are interested in analyzing a data set to determine if there are *any* cyclostationary signals present. No information about the received data is assumed in the general search problem. In the second problem, called the *known-cycle-frequency problem*, we have in mind a specific pure cycle frequency/order pair (β, n_0) and we attempt to determine if there is a signal present in the data corresponding to this pair. In the third problem, called the *known-modulation problem*, we know the modulation format of the signal of interest, and hence we know (in principle) the cyclic cumulants of the signal; we wish to determine if that particular signal is present.

Motivation for using HOCS, instead of SOCS or HOS, to detect the presence of a signal is provided by the situation where this detection cannot be reliably accomplished using these other signal properties. This can be the case, for example, when a signal has very weak SOCS, and is weak with respect to the noise and interference background (low SNR), which is changing unpredictably during the observation interval. It can also be the case when the signal of interest does not have a unique cycle frequency for order two, but does for a higher order. An example of this is a communication system wherein all the signals are spectrally overlapping QPSK and have the same symbol rate, but each has a distinct carrier frequency.

Since the computational complexity increases and the output SNR decreases (when the input SNR is less than 0dB) with increasing order n of nonlinearity, it is always desirable to use the smallest possible value of n. This typically corresponds to the lowest order of (substantial) cyclostationarity of the signal. Accordingly, it is often the case in the known-modulation problem that the CTCF and CTMF are (approximately) equal for the chosen value of n, $R_s^\alpha(\boldsymbol{\tau})_n = C_s^\alpha(\boldsymbol{\tau})_n$. In addition, if the noise and interference (hereafter referred to as the environment) is such that $R_n^\beta(\boldsymbol{\tau})_n = 0$, where β is the pure cycle frequency of interest in $s(t)$, in which case $R_x^\beta(\boldsymbol{\tau})_n = C_s^\beta(\boldsymbol{\tau})_n$, then any detection method that requires an estimate of the CTCF for $s(t)$ can be implemented by using an estimate of the CTMF for $x(t)$, thereby reducing the computational complexity of the method. However, if the environment is unknown, it is best to use estimates of the CTCF so that potential lower order sine wave interactions can be avoided. Let us now turn to an examination of each of the three detection problems.

1) The General Search Problem: In the general search problem, there is a maximum order N that is to be used for processing. The goal of the processing is to produce a list of pure cycle frequencies $\{\beta_n\}$ for each value of n from 1 to N. The list $\{\beta_n\}$ should characterize the detectable cyclostationarity of order n (and only n) that is associated with $x(t)$. Thus, these lists should not be contaminated by entries that are due to lower order sine-wave interactions. To accomplish this task, we estimate the TCF for $x(t)$ for each order n. From this estimate, the cycle frequencies $\{\beta_n\}$, which are needed for the estimate of the TCF for order $n+1$, can be found. More explicitly, the general search problem can be tackled using the following algorithm:

0. Let $n = 1$
1. $\hat{C}'_x(t,\boldsymbol{\tau})_n = L_x(t,\boldsymbol{\tau})_n - \sum_{\substack{P_n \\ p \ne 1}} \left[\prod_{j=1}^{p} \hat{C}_x(t,\boldsymbol{\tau}_{\nu_j})_{n_j} \right]$
2. $Y(f) = \mathrm{FFT}_t\{\hat{C}'_x(t,\boldsymbol{\tau})_n\}$
3. Threshold detect the bins of Y to find $\{\beta_n\}$

4. $\hat{C}_x^{\beta_n}(\boldsymbol{\tau})_n = \langle \hat{C}'_x(t,\boldsymbol{\tau})_n e^{-i2\pi\beta_n t}\rangle$
5. $\hat{C}_x(t,\boldsymbol{\tau})_n = \sum_{\beta_n} \hat{C}_x^{\beta_n}(\boldsymbol{\tau})_n e^{i2\pi\beta_n t}$
6. $n \rightarrow n+1$; if $n \leq N$ then go to 1.

In step 4, the interval over which the average $\langle\cdot\rangle$ is performed is determined by the amount of data $x(t)$ available. If any of the detected cycle frequencies are of particular interest, a cyclic polyspectral analysis can be performed from which the modulation type can possibly be determined. Also, a simple analysis of the relationship between the estimated cycle frequencies for the different values of n can be used to advantage for modulation recognition.

2) The Known-Cycle-Frequency Problem: Here we are given knowledge of one or more of the signal's modulation frequencies, such as a symbol rate or carrier frequency, but the shape of the CTCF is unknown. The environment is still assumed to be unknown and, therefore, the general search algorithm is still of interest. It can be improved for the known-cycle-frequency problem by combining it with a least-squares estimation technique. Let (β, n_0) be the cycle frequency/order pair of interest. Use the general search algorithm up to order $n_0 - 1$. Form $\hat{C}'_x(t,\boldsymbol{\tau})_{n_0}$ and use a least-squares estimator to detect the presence of the signal of interest using the statistic

$$\begin{aligned} Y &= \langle \hat{\boldsymbol{w}}^\dagger \hat{\boldsymbol{C}}'_x(t,\boldsymbol{\tau})_{n_0} e^{-i2\pi\beta t}\rangle \\ &= \hat{\boldsymbol{w}}^\dagger \hat{\boldsymbol{C}}_x^{\beta}(\boldsymbol{\tau})_{n_0}, \end{aligned}$$

where

$$\begin{aligned} \hat{\boldsymbol{C}}'_x(t,\boldsymbol{\tau})_{n_0} &= \left[\hat{C}'_x(t,\boldsymbol{\tau}_1)_{n_0} \cdots \hat{C}'_x(t,\boldsymbol{\tau}_K)_{n_0}\right]^\dagger \\ \hat{\boldsymbol{C}}_x^{\beta}(\boldsymbol{\tau})_{n_0} &= \left[\hat{C}_x^{\beta}(\boldsymbol{\tau}_1)_{n_0} \cdots \hat{C}_x^{\beta}(\boldsymbol{\tau}_K)_{n_0}\right]^\dagger \end{aligned}$$

and where $\hat{\boldsymbol{w}}$ is the unity-norm version of the least-squares weight vector that satisfies

$$\min_{\boldsymbol{w}} \langle |\boldsymbol{w}^\dagger \hat{\boldsymbol{C}}'_x(t,\boldsymbol{\tau})_{n_0} - e^{i2\pi\beta t}|^2\rangle. \tag{58}$$

The normalized solution to (58) is

$$\hat{\boldsymbol{w}} = \boldsymbol{R}^{-1}\hat{\boldsymbol{C}}_x^{\beta}(\boldsymbol{\tau})_{n_0} \parallel \boldsymbol{R}^{-1}\hat{\boldsymbol{C}}_x^{\beta}(\boldsymbol{\tau})_{n_0} \parallel^{-1}$$

where

$$\boldsymbol{R} = \langle \hat{\boldsymbol{C}}'_x(t,\boldsymbol{\tau})_{n_0} \hat{\boldsymbol{C}}'_x(t,\boldsymbol{\tau})_{n_0}^H\rangle$$

in which H denotes conjugate transpose. Thus, the detection statistic is

$$Y = \hat{\boldsymbol{C}}_x^{\beta}(\boldsymbol{\tau})_{n_0}^H \boldsymbol{R}^{-1} \hat{\boldsymbol{C}}_x^{\beta}(\boldsymbol{\tau})_{n_0} \left[\hat{\boldsymbol{C}}_x^{\beta}(\boldsymbol{\tau})_{n_0}^H \boldsymbol{R}^{-2} \hat{\boldsymbol{C}}_x^{\beta}(\boldsymbol{\tau})_{n_0}\right]^{-1/2}.$$

This detection statistic is obtained by forming the particular linear combination of data sets $\hat{\boldsymbol{C}}'(t,\boldsymbol{\tau}_1)_{n_0}, \ldots, \hat{\boldsymbol{C}}'(t,\boldsymbol{\tau}_K)_{n_0}$ that optimally combines the regenerated sine waves with frequency β present in each set, and then correlates this composite regenerated sine wave with the stored sine wave $e^{i2\pi\beta t}$.

3) The Known-Modulation Problem: In this problem, we wish to determine if a signal with known modulation type is present. In particular, we know the CTCF of $s(t)$ for $n = n_0$ and pure cycle frequency β. The general search algorithm can be used to remove all lower order sine waves up to order $n_0 - 1$. Then, from $\hat{C}'_x(t,\boldsymbol{\tau})_{n_0}$ the CTCF estimate $\bar{C}_{x_T}^{\beta}(\boldsymbol{u})_{n_0}$ for cycle frequency β can be determined. The proposed detection statistic is

$$Y = \int_{-\infty}^{\infty} \cdots \int_{-\infty}^{\infty} \bar{C}_{x_T}^{\beta}(\boldsymbol{u})_{n_0} \bar{C}_s^{\beta}(\boldsymbol{u})_{n_0}^* d\boldsymbol{u}.$$

The primary justification for this particular statistic is that when no signal is present with pure nth-order cycle frequency β, then $\bar{C}_{x_T}^{\beta}(\boldsymbol{u})_{n_0} \rightarrow 0$, which implies that $Y \rightarrow 0$; when the signal of interest is present, then

$$Y \rightarrow \int_{-\infty}^{\infty} \cdots \int_{-\infty}^{\infty} \left|\bar{C}_s^{\beta}(\boldsymbol{u})_n\right|^2 d\boldsymbol{u}. \tag{59}$$

Thus, y is an asymptotically noise-free statistic on both the signal-present and signal-absent hypotheses. (Furthermore, the integral (59) is finite (see Part I, Section II).) Hence, this statistic is the natural generalization of the single cycle detector that exploits second-order cyclostationarity [11]

$$Y_{\text{SCD}} = \int_{-\infty}^{\infty} R_{x_T}^{\alpha}(\tau) R_s^{\alpha}(\tau)^* d\tau = \int_{-\infty}^{\infty} S_{x_T}^{\alpha}(f) S_s^{\alpha}(f)^* df \tag{60}$$

which has several optimality properties [12] and has been shown to outperform radiometric (energy) detectors for weak cyclostationary signals in time-varying environments [15]. In (60), $R_s^{\alpha}(\tau)$ is the cyclic autocorrelation for $s(t)$, $R_{x_T}^{\alpha}(\tau)$ is the cyclic autocorrelation estimate (cyclic correlogram), $S_{x_T}^{\alpha}(f)$ is the cyclic periodogram, and $S_s^{\alpha}(f)$ is the cyclic spectrum for $s(t)$ [34].

The detection statistic Y can be generalized to include only a portion of $\boldsymbol{u}$-space, denoted by $G \subset \boldsymbol{R}^{n_0}$

$$Y = \int_G \bar{C}_{x_T}^{\beta}(\boldsymbol{u})_{n_0} \bar{C}_s^{\beta}(\boldsymbol{u})_{n_0}^* d\boldsymbol{u}.$$

Choices for G might include those values of $\boldsymbol{u}$ for which the RD-CTCF $\bar{C}_s^{\beta}(\boldsymbol{u})_{n_0}$ is particularly large, or for which the coefficient of variation (variance divided by squared mean) of the estimator $\bar{C}_{x_T}^{\beta}(\boldsymbol{u})_{n_0}$ of the RD-CTCF is particularly small.

B. Time-Delay Estimation

In this section, we consider the problem of time-delay estimation. We are given the data

$$\begin{aligned} x(t) &= s(t) + n(t) \\ y(t) &= As(t+d) + m(t) \end{aligned}$$

from two physically separated sensors and we wish to estimate the time-delay parameter d, which is sometimes called the time-difference-of-arrival (TDOA) for $s(t)$. We assume that $s(t)$ is nth-order cyclostationary with cycle frequency β. The time-series $n(t)$ and $m(t)$ consist of arbitrary noise and interfering signals, except that it is assumed that neither $n(t)$ nor $m(t)$ is nth-order cyclostationary with the pure nth-order cycle frequency β.

Conventional approaches to this problem (those that do not exploit cyclostationarity) can be collectively referred to as *generalized cross-correlation* (GCC) methods [25]. In the GCC methods, filtered versions of the sensor outputs $x(t)$ and $y(t)$ are cross-correlated, and the estimate of d is taken to be the location of the peak in the cross-correlation estimate. These methods suffer when $n(t)$ and $m(t)$ contain signals common to both, each with its own TDOA, because each such signal contributes a peak of its own to the cross-correlation function. This causes two problems. The first is a resolution problem which, to be solved, requires that the differences in the TDOA's for each of the signals be greater than the widths of the cross-correlation functions so that the peaks can be resolved. The second problem is that it is difficult to correctly associate each peak with its corresponding signal. Both of these problems arise because the GCC methods are not signal selective; they produce TDOA peaks for all the signals in the received data unless they are spectrally disjoint and can, therefore, be separated by filtering. Signal selective methods that exploit the SOCS of the desired signal, which is assumed to be unique to that signal, are studied in [8], [16], and [17]. These methods have been shown to outperform the GCC methods, and have been shown to produce unbiased TDOA estimates with variance that is smaller than the Cramér-Rao lower bound on the variance of TDOA estimators that are based on the assumption that the signal and environment are stationary. However, these methods do not apply when there is no SOCS to exploit. In this case, we can turn to HOCS in order to develop signal-selective TDOA estimators.

Following the approach in [16] for SOCS, the general methodology considered here for HOCS is least-squares estimation [33]. The following two examples illustrate the methodology. To keep the notation simple only real-valued signals are considered.

Let us define a cross-cumulant as

$$C_{\boldsymbol{x}y}(t,\boldsymbol{\tau})_n \triangleq \text{Cumulant}\{x(t+\tau_1)\cdots x(t+\tau_{n-1})\; y(t+\tau_n)\}.$$

The cyclic component of this cross-cumulant for the signal-specific cycle frequency β is

$$\begin{aligned} C^{\beta}_{\boldsymbol{x}y}(\boldsymbol{\tau})_n &\triangleq \langle C_{\boldsymbol{x}y}(t,\boldsymbol{\tau})_n e^{-i2\pi\beta t}\rangle \\ &= AC^{\beta}_s(\boldsymbol{\tau}+\boldsymbol{\delta}_n d)_n \end{aligned}$$

where $\boldsymbol{\delta}_n$ is the unit vector along the nth coordinate. It is easy to show that the following relations involving RD-CTCF's hold:

$$\begin{aligned} \bar{C}^{\beta}_{\boldsymbol{x}y}(\boldsymbol{u})_n &= A\bar{C}^{\beta}_s(\boldsymbol{u}-\mathbf{1}d)_n e^{i2\pi\beta d}, \\ \bar{C}^{\beta}_x(\boldsymbol{u})_n &= \bar{C}^{\beta}_s(\boldsymbol{u})_n. \end{aligned}$$

Thus, we can do a least-squares fit of a measurement of $\bar{C}^{\beta}_{\boldsymbol{x}y}$ to a measurement of $\bar{C}^{\beta}_x$ over a region G of $\boldsymbol{u}$-space of interest:

$$\min_{A,\hat{d}} \int_G \left|\bar{C}^{\beta}_{\boldsymbol{x}yT}(\boldsymbol{u})_n - A\bar{C}^{\beta}_{x_T}(\boldsymbol{u}-\mathbf{1}\hat{d})_n e^{i2\pi\beta\hat{d}}\right|^2 d\boldsymbol{u}.$$

This leads (cf. [16]) to the following estimator of the delay d:

$$\hat{d}_1 = \arg\max_{\hat{d}} \Re \int_G \bar{C}^{\beta}_{x_T}(\boldsymbol{u})_n \bar{C}^{\beta}_{\boldsymbol{x}y_T}(\boldsymbol{u}+\mathbf{1}\hat{d})^*_n e^{i2\pi\beta\hat{d}} d\boldsymbol{u}$$

where arg max means the value at which the maximum occurs, and $\Re$ means the real part. This estimator is a higher order generalization of the spectral coherence alignment (SPECCOA) algorithm for TDOA estimation [16], which exploits second-order cyclostationarity, and has been shown to possess several optimality properties [40].

As an alternative, we can avoid using cross-sensor measurements entirely by noting that

$$\bar{C}^{\beta}_y(\boldsymbol{u})_n = A^n \bar{C}^{\beta}_s(\boldsymbol{u})_n e^{i2\pi\beta d}$$

and

$$\bar{C}^{\beta}_x(\boldsymbol{u})_n = \bar{C}^{\beta}_s(\boldsymbol{u})_n$$

which suggests the following least-squares approach:

$$\hat{d}_2 = \arg\min_{A,\hat{d}} \int_G \left|\bar{C}^{\beta}_{y_T}(\boldsymbol{u})_n - A^n \bar{C}^{\beta}_{x_T}(\boldsymbol{u})_n e^{i2\pi\beta\hat{d}}\right|^2 d\boldsymbol{u}.$$

The estimator for d is given explicitly by

$$\hat{d}_2 = \frac{-1}{2\pi\beta}\text{angle}\left\{\int_G \bar{C}^{\beta}_{x_T}(\boldsymbol{u})_n \bar{C}^{\beta}_{y_T}(\boldsymbol{u})^*_n d\boldsymbol{u}\right\}$$

which is a higher order generalization of the second-order cyclic phase difference (CPD) algorithm for TDOA estimation without cross-sensor measurements [16]. When generalized to more than two sensors, CPD becomes a form of cyclic MUSIC for high-resolution direction finding [41], [42]. This suggests that similar methods of high-resolution direction finding with higher order statistics could be obtained by generalizing the higher order CPD algorithm.

In general, there are as many estimators of the TDOA as there are ways of choosing l $x(t+\tau)$-type terms and $n-l$ $y(t+\tau)$-type terms. Thus, for large n there are many different possibilities. The relative advantages and disadvantages of these possibilities are currently being sought. The individual statistics can also be combined using a least-squares technique, as is done for order two in [8].

VIII. Concluding Remarks

In this paper, we generalize the basic parameters of higher order cyclostationarity (HOCS) from real-valued to complex-valued time-series and derive input-output relations for these statistical parameters for various signal processing operations; we use these relations and examine this generalization in detail for the class of digital QAM signals, and we apply the parameters of HOCS to some signal processing problems of current interest, namely weak-signal detection and time-delay estimation. Several HOCS-parameter estimation methods are presented and demonstrated for digital QAM signals in noise and interference, and some potential pitfalls in the application of the conventional theory of higher order statistics (HOS) to modulated signals that are modeled as stationary but not cycloergodic are explained.

We are currently developing HOCS-based algorithms for the problems of cochannel interference mitigation [36], weak-signal detection in variable noise and interference backgrounds, time-delay estimation for weak signals [33], and multiple signal detection, sorting, and classification [43],

and we are applying the theory of HOCS to the design of covert signals.

APPENDIX A
A NEW TYPE OF CUMULANT FOR COMPLEX-VALUED RANDOM VARIABLES

In this Appendix, we show how to define cumulants directly for complex-valued random variables in terms of a generalized characteristic function for complex random variables (even though PDF's can be defined *only* in terms of the real and imaginary parts). Prior to this, cumulants have apparently been defined only for the real and imaginary parts of the complex random variables, which are defined in terms of the usual characteristic functions for real random variables, or they were defined only through the moment/cumulant relationship [34]. This new definition is necessary in order to be able to characterize pure nth-order sine waves in terms of cumulants.

For the set of real-valued random variables $\{X_j\}_{j=1}^n$, the joint PDF is the n-fold derivative of the probability distribution function

$$f_{\boldsymbol{X}}(\boldsymbol{x}) \triangleq \frac{\partial^n}{\partial x_1 \cdots \partial x_n} F_{\boldsymbol{X}}(\boldsymbol{x})$$

where

$$F_{\boldsymbol{X}}(\boldsymbol{x}) \triangleq \text{ Prob}\left\{\bigcap_{j=1}^n X_j < x_j\right\}.$$

The moments of $\{X_j\}_{j=1}^n$ can be found by differentiating the characteristic function:

$$\Phi_{\boldsymbol{X}}(\boldsymbol{\omega}) \triangleq E\left\{\exp\left(i\sum_{j=1}^n x_j\omega_j\right)\right\}.$$

Specifically

$$E\left\{\prod_{j=1}^n X_j\right\} = (i)^{-n}\frac{\partial^n}{\partial\omega_1\cdots\partial\omega_n}\Phi_X(\boldsymbol{\omega})\bigg|_{\boldsymbol{\omega}=\mathbf{0}}.$$

Other moments can be found by other derivatives, for example, $E\{X_k^m\}$ is given by

$$E\{X_k^m\} = (i)^{-m}\frac{\partial^m}{\partial\omega_k^m}\Phi_{\boldsymbol{X}}(\omega)|_{\omega=\mathbf{0}}.$$

For complex-valued variables, the situation is a little different. The n complex-valued variables $\{Y_j\}_{j=1}^n$ must be be viewed as $2n$ real-valued variables in order to obtain a PDF. However, a generalized characteristic function for $\{Y\}_{j=1}^n$ can be defined in terms of the $2n$-fold PDF corresponding to the $2n$ real variables $\{\Re(Y_j), \Im(Y_j)\}_{j=1}^n \equiv \{Z_j\}_{j=1}^{2n}$ consisting of the real and imaginary parts of $\{Y_j\}_{j=1}^n$:

$$\begin{aligned}\Phi_{\boldsymbol{Y}}(\boldsymbol{\omega}) &= E\left\{\exp\left(i\sum_{j=1}^n Y_j\omega_j\right)\right\}\\ &= \underbrace{\int_{-\infty}^{\infty}\cdots\int_{-\infty}^{\infty}}_{2n}\exp\left(i\sum_{j=1}^n y_j\omega_j\right)f_{\boldsymbol{Z}}(\boldsymbol{z})d\boldsymbol{z}\\ &= \int_{-\infty}^{\infty}\cdots\int_{-\infty}^{\infty}\exp\left(i\sum_{j=1}^n [z_j+iz_{j+n}]\omega_j\right)f_{\boldsymbol{Z}}(\boldsymbol{z})d\boldsymbol{z}\end{aligned}$$

where

$$\boldsymbol{Z} \triangleq [\Re(Y_1)\cdots\Re(Y_n)\ \Im(Y_1)\cdots\Im(Y_n)].$$

This multiple integral exists if the integrand is absolutely integrable, but the integral of the absolute value of the integrand simplifies to

$$\underbrace{\int_{-\infty}^{\infty}\cdots\int_{-\infty}^{\infty}}_{n}\prod_{j=1}^n \exp(-I(y_j)\omega_j)f_{I(\boldsymbol{Y})}(I(\boldsymbol{y}))dI(\boldsymbol{y}) \quad (61)$$

where $I(y_j) = z_{j+n}$; and for every finite ω, this integral exists if the PDF for the vector of imaginary components $f_{I(\boldsymbol{Y})}$ of the complex vector $\boldsymbol{Y}$ decays more rapidly than

$$\prod_{j=1}^n \frac{1}{|I(y_j)|}\exp(-|I(y_j)\omega|).$$

Few PDF's of interest do not decay this rapidly. For example, all Gaussian PDF's and all PDF's with finite support do decay this rapidly. As a counterexample, the Cauchy PDF does not decay this rapidly, but its variance does not even exist. Similarly, all PDF's for which some moments do not exist do not decay this rapidly. But we are not interested in such PDF's because their corresponding cumulants would not exist either.

Now, the moments of the Y_j can be found by differentiating $\Phi_{\boldsymbol{Y}}(\boldsymbol{\omega})$. For example

$$\begin{aligned}E[Y_k] &= (i)^{-1}\frac{\partial}{\partial\omega_k}\Phi_{\boldsymbol{Y}}(\boldsymbol{\omega})|_{\boldsymbol{\omega}=0}\\ &= (i)^{-1}(i)\underbrace{\int_{-\infty}^{\infty}\cdots\int_{-\infty}^{\infty}}_{2n}[z_k+iz_{k+n}]f_{\boldsymbol{Z}}(\boldsymbol{z})d\boldsymbol{z}\\ &= \int_{-\infty}^{\infty}\int_{-\infty}^{\infty}[z_k+iz_{k+n}]f_{Z_k,Z_{k+n}}(z_k,z_{k+n})dz_k dz_{k+n}\\ &\equiv E\{Z_k+iZ_{k+n}\}.\end{aligned}$$

In addition, the joint moments of the real and imaginary parts of the Y_j can be found similarly by first expressing these parts as

$$\begin{aligned}R\{Y_j\} &= \frac{1}{2}(Y_j+Y_j^*)\\ I\{Y_j\} &= \frac{1}{2i}(Y_j-Y_j^*)\end{aligned}$$

and then using this to express the joint moment for $R(Y_j)$ and $I(Y_j)$ in terms of a joint moment, including conjugations, of

Y_j and then using the generalized characteristic function for the Y_j including conjugations.

The function $\Phi_{\boldsymbol{Y}}(\boldsymbol{\omega})$ can be expanded into a Taylor series where the various coefficients are the various joint moments of the Y_j. Since the relationship between the coefficients of this series and the series expansion of $\ln \Phi_{\boldsymbol{Y}}(\boldsymbol{\omega})$ is purely algebraic, and this algebraic relation is that between moments and conventional cumulants, then the cumulants of $\{Y_j\}$, defined here in terms of moments using the same cumulant-moment relation that holds for real variables, are given by the Taylor series coefficients of $\ln \Phi_{\boldsymbol{Y}}(\boldsymbol{\omega})$, which can be obtained by differentiation and evaluation at $\boldsymbol{\omega} = \mathbf{o}$.

Conversely, if we use the generalized characteristic function introduced here, and define cumulants for complex variables in direct analogy to the definition in terms of the conventional characteristic function for real variables, then we obtain a moment-cumulant relation for complex variables that is identical to that for real variables, in which case the temporal cumulant function for a complex time-series is identical to the pure-sine-waves function for that time-series.

It is mentioned in closing that the cumulants defined here cannot in general be expressed directly in terms of cumulants of real and imaginary parts, and vice versa. This can only be done through the expression of moments of one in terms of the other, and is very complicated. Thus, the conventional approach to cumulants of complex variables [26], [28], [29] is not useful in the study of pure nth-order sine waves of complex-valued polycyclostationary time-series unless one is interested in the real and imaginary parts individually rather than in the complex time-series as a whole.

Appendix B
Mean and Variances of Temporal Moment Estimates

In this section, some results on the mean and variance of the RD-CTMF estimate $\bar{R}^{\alpha}_{x_T}(t,\boldsymbol{u})_n$ are presented and discussed. The derivation of the results is contained in [35].

The temporal variance for a cyclostationary time-series is defined in terms of the sine-wave extraction operation

$$\mathrm{Var}\{x(t)\} \triangleq \hat{E}^{\{\alpha\}}\{|x(t) - \hat{E}^{\{\alpha\}}\{x(t)\}|^2\} \tag{62}$$

and it is time-varying. The time-averaged variance is the $\alpha = 0$ component of the variance

$$\begin{aligned}\mathrm{Var}_0\{x(t)\} &\triangleq \langle |x(t) - \hat{E}^{\{\alpha\}}\{x(t)\}|^2\rangle \\ &= \langle |x(t)|^2\rangle - \langle |\hat{E}^{\{\alpha\}}\{x(t)\}|^2\rangle. \end{aligned}\tag{63}$$

The variance formula (62) can result in very complicated analyses. For this reason, and the assumption that the time-averaged temporal variance captures the essential behavior of the temporal variance, the time-averaged variance (63) is focused on herein.

It can be shown that the time-varying mean of the RD-CTMF estimate is given by [35]

$$\begin{aligned}&\hat{E}^{\{\alpha\}}\{\bar{R}^{\alpha}_{x_T}(t,\boldsymbol{u})_n\} = \\ &\quad \frac{1}{T}\bar{R}^{\alpha}_{x}(\boldsymbol{u})_n(u_0^* + T) + \frac{1}{T}\sum_{a\neq\alpha}\Big[\bar{R}^{a}_{x}(\boldsymbol{u})_n e^{-i\pi[\alpha-a](u_l+u_r)} \\ &\qquad \times (u_0^* + T)\mathrm{sinc}([\alpha - a]\times(u_0^* + T))e^{-i2\pi[\alpha-a]t}\Big] \end{aligned}\tag{64}$$

where

$$\begin{aligned} u_l &\triangleq -\min\{0, u_1, \ldots, u_{n-1}\}, \\ u_r &\triangleq -\max\{0, u_1, \ldots, u_{n-1}\}, \\ u_0^* &\triangleq u_r - u_l. \end{aligned}$$

Formula (64) reveals that the temporal mean of the CTMF estimate contains a sine-wave component for each impure nth-order cycle frequency that is associated with $x(t)$.

It is shown in [35] that the time-averaged variance for $\bar{R}^{\alpha}_{x_T}(t,\boldsymbol{u})_n$ is given by

$$\begin{aligned}\mathrm{Var}_0\{\bar{R}^{\alpha}_{x_T}(t,\boldsymbol{u})_n\} = \sum_{P'_n}\Bigg[\int_{-u_0^*-T}^{u_0^*+T}\sum_{\boldsymbol{\beta}^\dagger\mathbf{1}=0}\prod_{j=1}^{p} C_x^{\beta_j}(\hat{\boldsymbol{w}}_{n_j})_{n_j} \\ \times\left(\frac{u_0^* - |z| + T}{T^2}\right)e^{-i2\pi\alpha z}dz\Bigg] \end{aligned}\tag{65}$$

where P'_n is a subset of the partitions of the index set $\{1,2,\ldots,2n\}$ such that for each member of P'_n, at least one partition element, say ν_k, contains at least one element from $\{1,2,\ldots,n\}$ and at least one element from $\{n+1, n+2,\cdots,2n\}$, and

$$\begin{aligned}\hat{\boldsymbol{w}} &\triangleq [u_1 + z/2\cdots u_{n-1} + z/2 \;\; z/2 \\ &\qquad u_1 - z/2\cdots u_{n-1} - z/2 \;\; -z/2]^\dagger \\ &= [\hat{w}_1\cdots\hat{w}_{2n}]^\dagger. \end{aligned}$$

Before specializing (65) to the cases of $n = 2$, Gaussian time-series, and stationary time-series, the temporal covariance between estimates of the CTMF is given. The time-averaged temporal covariance is defined by

$$\begin{aligned}&\mathrm{Cov}_0\{\bar{R}^{\alpha}_{x_T}(t,\boldsymbol{u})_n, \bar{R}^{\alpha}_{x_T}(t,\boldsymbol{v})_n\} \\ &\quad \triangleq \langle \bar{R}^{\alpha}_{x_T}(t,\boldsymbol{u})_n \bar{R}^{\alpha}_{x_T}(t,\boldsymbol{v})^*_n\rangle \\ &\qquad - \langle \hat{E}^{\{\alpha\}}\{\bar{R}^{\alpha}_{x_T}(t,\boldsymbol{u})_n\}\hat{E}^{\{\alpha\}}\{\bar{R}^{\alpha}_{x_T}(t,\boldsymbol{v})^*_n\}\rangle \end{aligned}$$

and it is shown in [35] that it is given by

$$\begin{aligned}\mathrm{Cov}_0 &= \frac{1}{T^2}\bar{R}^{\alpha}_{x}(\boldsymbol{u})_n\bar{R}^{\alpha}_{x}(\boldsymbol{v})^*_n\left[(\tau_0^*+T)^2 - (u_0^*+T)(v_0^*+T)\right] \\ &\quad + \frac{1}{T^2}\sum_{a\neq\alpha}\bar{R}^{a}_{x}(\boldsymbol{u})_n\bar{R}^{a}_{x}(\boldsymbol{v})^*_n[(\tau_0^*+T)^2 \\ &\qquad \times \mathrm{sinc}^2([a-\alpha](\tau_0^*+T)) \\ &\quad - e^{-i\pi[a-\alpha](u_l+u_r-v_l-v_r)}(u_0^*+T)(v_0^*+T) \\ &\qquad \times \mathrm{sinc}([a-\alpha](u_0^*+T))\mathrm{sinc}([a-\alpha](v_0^*+T))] \\ &\quad + \sum_{P'_n}\Bigg[\int_{-\tau_0^*-T}^{\tau_0^*+T}\sum_{\boldsymbol{\beta}^\dagger\mathbf{1}=0}\prod_{j=1}^{p} C_x^{\beta_j}(\boldsymbol{w}_{\nu_j})_{n_j} \\ &\qquad \times\left(\frac{\tau_0^* - |z| + T}{T^2}\right)e^{-i2\pi\alpha z}dz\Bigg] \end{aligned}\tag{66}$$

where P_n' is the same as in (65), and

$$\begin{aligned}
\boldsymbol{w} &\triangleq [u_1 + z/2 \cdots u_{n-1} + z/2 \;\; z/2 \;\; v_1 - z/2 \cdots \\
&\qquad \cdots v_{n-1} - z/2 \;\; -z/2]^\dagger \\
&= [w_1 \cdots w_{2n}]^\dagger \\
U_r &\triangleq -\max\{0, u_j, v_j{:}1 \le j \le n-1\} \\
U_l &\triangleq -\min\{0, u_j, v_j{:}1 \le j \le n-1\} \\
\tau_0^* &\triangleq U_r - U_l \\
v_r &\triangleq -\max\{0, v_j{:}\, 1 \le j \le n-1\} \\
v_l &\triangleq -\min\{0, v_j{:}\, 1 \le j \le n-1\} \\
v_0^* &\triangleq v_r - v_l.
\end{aligned} \tag{67}$$

Note that the covariance (66) reduces to the variance (65) in the case of $\boldsymbol{u} = \boldsymbol{v}$ because in this case $\tau_0^* = u_0^* = v_0^*$ and $\hat{\boldsymbol{w}} = \boldsymbol{w}$. The variance formula (65) is specialized to the simple cases of $n = 2$, Gaussian time-series, and stationary time-series in the following section.

Special Variances: The time-series $x(t)$ is assumed to have a mean of zero. In the case of $n = 2$, the sum over P_n' is the sum over the following partitions of $\{1, 2, 3, 4\}$:

$$\{1,2,3,4\} \quad \{1,3\}\{2,4\} \quad \{1,4\}\{2,3\}.$$

Therefore, (65) yields

$$\begin{aligned}
\mathrm{Var}_0\{\hat{R}^\alpha_{x_T}(t,u_1)_2\} = &\int_{-u_0^*-T}^{u_0^*+T} C_x^0(\hat{\boldsymbol{w}})_4 \left(\frac{u_0^* - |z| + T}{T^2}\right) \\
&\times e^{-i2\pi\alpha z} dz \\
&+ \int_{-u_0^*-T}^{u_0^*+T} \left[\sum_\beta C_x^\beta(u_1 + z/2, u_1 - z/2)_2 \right. \\
&\times C_x^{-\beta}(z/2, -z/2)_2 \\
&+ C_x^\beta(u_1 + z/2, -z/2)_2 \\
&\left. \times C_x^{-\beta}(z/2, u_1 - z/2)_2 \right] \\
&\times \left(\frac{u_0^* - |z| + T}{T^2}\right) e^{-i2\pi\alpha z} dz.
\end{aligned} \tag{68}$$

If $x(t)$ is a Gaussian time-series, then the fourth-order cyclic cumulant $C_x^0(\cdot)_4$ is identically zero. Thus, the variance of the second-order CTMF for a Gaussian time-series is (68) with the first integral deleted, which matches Hurd's result in [23] on the variance of the cyclic autocorrelation for Gaussian stochastic processes. This illustrates that the time-average framework used here does indeed yield the same results as those obtained within the stochastic process framework.

If $x(t)$ is a wide-sense stationary time-series, then the variance expression simplifies to

$$\begin{aligned}
&\mathrm{Var}_0\{\hat{R}^0_{x_T}(t,u_1)_2\} \\
&\quad = \int_{-u_0^*-T}^{u_0^*+T} \left[C_x^0(\hat{\boldsymbol{w}})_4 + C_x^0(u_1 + z/2, u_1 - z/2)_2 \right. \\
&\qquad \times C_x^0(z/2, -z/2)_2 + C_x^0(u_1 + z/2, -z/2)_2 \\
&\qquad \left. \times C_x^0(z/2, u_1 - z/2)_2 \right] \left(\frac{u_0^* - |z| + T}{T^2}\right) dz.
\end{aligned}$$

The variance of the CTCF estimate is much more complicated, and is not pursued herein. However, in the case that the CTMF and CTCF are equal, then the variance expressions derived here apply to the CTCF as well. In addition, methods of CP estimation that make use of the RD-CTMF or its transform, the cyclic periodogram, can be statistically analyzed by using the covariance (66).

REFERENCES

[1] D. R. Brillinger, "An introduction to polyspectra," *Ann. Math. Stat.*, vol. 36, pp. 1351–1374, 1965.

[2] D. R. Brillinger and M. Rosenblatt, "Asymptotic theory of estimates of k-th order spectra," in *Spectral Analysis of Time Series,* B. Harris, Ed. New York: Wiley 1967.

[3] ——, "Computation and interpretation of k-th order spectra," in *Spectral Analysis of Time Series,* B. Harris, Ed. New York: Wiley 1967.

[4] H.-H. Chiang and C. L. Nikias, "A new method for adaptive time delay estimation for non-Gaussian signals," *IEEE Trans. Signal Processing,* vol. 38, no. 2, pp. 209–219, Feb. 1990.

[5] A. V. Dandawate and G. B. Giannakis, "Ergodicity results for non stationary signals: Cumulants, ambiguity functions and wavelets," in *Proc. 25th Ann. Conf. Inform. Sci., Syst.* (Johns Hopkins University, Baltimore), Mar. 20–22, 1991, pp. 976–983.

[6] ——, "Nonparametric polyspectral analysis of AM signals and processes with missing observations," in *Proc. 26th Conf. Inform. Sci., Syst.* (Princeton University, NJ), March 18–20, 1992.

[7] ——, "Detection and classification of cyclostationary signals using cyclic-HOS: A unified approach," in *Proc. Soc. Photo-Opt. Instr. Engr., Adv. Signal Processing Algorithms, Architectures, Implementat.* (San Diego, CA), July 1992.

[8] G. Fong, W. A. Gardner, and S. V. Schell, "An algorithm for improved signal-selective time-difference estimation for cyclostationary signals," *IEEE Signal Processing Letts.*, vol. 1, No. 2, 1994.

[9] W. A. Gardner, "Stationarizable Random Processes," *IEEE Trans. Inform. Theory,* vol. IT–24, no. 1, pp. 8–22, 1978.

[10] ——, *Introduction to Random Processes with Applications to Signals and Systems.* New York: Macmillan, 1985 (2nd ed.: New York: McGraw-Hill, 1990).

[11] ——, *Statistical Spectral Analysis: A Non-Probabilistic Theory.* Englewood Cliffs, NJ: Prentice-Hall, 1987.

[12] ——, "Signal interception: A unifying theoretical framework for feature detection," *IEEE Trans. Commun.,* vol. 36, no. 8, pp. 897–906, Aug. 1988.

[13] W. A. Gardner and W. A. Brown, "Fraction-of-time probability for time-series that exhibit cyclostationarity," *Signal Processing,* vol. 23, no. 3, pp. 273–292, June 1991.

[14] W. A. Gardner, "Exploitation of spectral redundancy in cyclostationary signals," *IEEE Signal Processing Mag.,* vol. 8, no. 2, pp. 14–36, Apr. 1991.

[15] W. A. Gardner and C. M. Spooner, "Signal interception: Performance advantages of cyclic-feature detectors," *IEEE Trans. Commun.,* vol. 40, no. 1, pp. 149–159, Jan. 1992.

[16] W. A. Gardner and C. K. Chen, "Signal-selective time-difference-of-arrival estimation for passive location of manmade signal sources in highly corruptive environments, Part I: Theory and method," *IEEE Trans. Signal Processing,* vol. 40, no. 5, pp. 1168–1184, May 1992.

[17] C. K. Chen and W. A. Gardner, "Signal-selective time-difference-of-arrival estimation for passive location of manmade signal sources in highly corruptive environments, Part II: Algorithms and performance," *IEEE Trans. Signal Processing,* vol. 40, no. 5, pp. 1185–1197, May 1992.

[18] G. B. Giannakis and M. K. Tsatsanis, "Signal detection and classification using matched filtering and higher order statistics," *IEEE Trans. Acoust., Speech, Signal Processing,* vol. 38, no. 7, pp. 1284–1296, July 1990.

[19] G. B. Giannakis and A. V. Dandawate, "Polyspectral analysis of non-stationary signals: Bases, consistency and HOS-WV," *Proc. Int. Signal Processing Workshop Higher Order Stat.* (Chamrousse, France), July 10–12, 1991, pp. 167–170.
[20] ——, "Polyspectral analysis of (almost) cyclostationary signals: LPTV system identification and related applications," in *Proc. 25th Asilomar Conf. Signals, Syst., Comput.* (Pacific Grove, CA), November 4–6, 1991, pp. 377–382,
[21] G. B. Giannakis and S. Shamsunder, "Non-Gaussian source localization via exploitation of higher order cyclostationarity," in *6th Workshop Stat. Signal, Array Processing* (Victoria, BC, Canada), Oct. 7–9, 1992, pp. 193–196.
[22] M. J. Hinich and G. R. Wilson, "Time delay estimation using the cross bispectrum," *IEEE Trans. Signal Processing,* vol. 40, no. 1, pp. 106–113, Jan. 1992.
[23] H. L. Hurd, "Nonparametric time series analysis for periodically correlated processes," *IEEE Trans. Inform. Theory,* vol. 35, no. 2, pp. 350–359, Mar. 1989.
[24] D. Kletter and H. Messer, "Suboptimal detection of non-Gaussian signals by third-order spectral analysis," *IEEE Trans. Acoust., Speech, Signal Processing,* vol. 38, no. 6, pp. 901–909, June 1990.
[25] C. H. Knapp and G. C. Carter, "The generalized correlation method for estimation of time delay," *IEEE Trans. Acoust., Speech, Signal Processing*, vol. 24, no. 4, pp. 320–327, Aug. 1976.
[26] J. M. Mendel, "Tutorial on higher order statistics (spectra) in signal processing and system theory: Theoretical results and some applications," *Proc. IEEE,* vol. 79, no. 3, pp. 277–305, Mar. 1991.
[27] C. L. Nikias and M. R. Raghuveer, "Bispectrum estimation: A digital signal processing framework," *Proc. IEEE,* vol. 75, no. 7, pp. 869–891, July 1987.
[28] C. L. Nikias and A. P Petropulu, *Higher order Spectra Analysis.* Englewood Cliffs, NJ: Prentice-Hall, 1993.
[29] M. Rosenblatt, *Stationary Sequences and Random Fields.* Boston: Birkhauser, 1985.
[30] M. B. Priestley, *Non-Linear and Non-Stationary Time Series Analysis.* London: Academic, 1988.
[31] C. M. Spooner and W. A. Gardner, "Estimation of cyclic polyspectra," *Proc. 25th Ann. Asilomar Conf. Signals, Systems, Comput.* (Pacific Grove, CA), Nov. 4–6, 1991, pp. 370–376.
[32] ——, "Performance evaluation of cyclic polyspectrum estimators," *Proc. 26th Annual Asilomar Conf. Signals, Systems, Comput.* (Pacific Grove, CA), Oct. 26–28, 1992, pp. 477–483.
[33] ——, "Exploitation of higher order cyclostationarity for weak-signal detection and time-delay estimation," *Proc. 6th Workshop Stat. Signal, Array Processing* (Victoria, BC, Canada), Oct. 7–9, 1992, pp. 197–201.
[34] W. A. Gardner and C. M. Spooner, "The cumulant theory of cyclostationary time-series, Part I: Foundation," *IEEE Trans. Signal Processing,* this issue.
[35] C. M. Spooner, "Theory and application of higher order cyclostationarity," Ph.D. Dissertation, Dept. Elec., Comput. Eng., Univ. of CA, Davis, June 1992.
[36] C. M. Spooner and W. A. Gardner, "Cubic frequency-shift filtering for cochannel interference removal," *Proc. Int. Symp. Nonlinear Theory, Applicat.* (Honolulu), Dec. 5–9, 1993.
[37] W. Zhang and M. Raghuveer, "Nonparametric bispectrum-based time-delay estimators for multiple sensor data," *IEEE Trans. Signal Processing,* vol. 39, no. 3, pp. 770–774, Mar. 1991.
[38] I. G. Zhurbenko, "Statistical estimation of higher order spectra," *Theory of Probability, Applicat.,* vol. 30, pp. 75–86, 1985.
[39] W. A. Gardner, "An introduction to cyclostationary signals," in *Cyclostationarity in Communications and Signal Processing* (W. A. Gardner, Ed.). New York: IEEE, 1994, Ch. 1.
[40] W. A. Gardner and C. M. Spooner, "Detection and source location of weak cyclostationary signals: Simplifications of the maximum-likelihood receiver," *IEEE Trans. Commun.*, vol. 41, no. 6, pp. 905–916, June 1993.
[41] G. Xu and T. Kailath, "Direction-of-arrival estimation via exploitation of cyclostationarity—A combination of temporal and spatial processing," *IEEE Trans. Signal Processing*, vol. 40, no. 7, pp. 1775–1785, July 1992.
[42] S. V. Schell, "An overview of sensor array processing for cyclostationary signals," in *Cyclostationarity in Communications and Signal Processing* (W. A. Gardner, Ed.). New York: IEEE, 1994, Ch. 3.
[43] C. M. Spooner, "An overview of recent developments in cyclostationary signal processing," in *Proc. 2nd Workshop Cyclostationary Signals* (Monterey, CA), Aug. 1–2, 1994, pp. 1.1–1.17.

Chad M. Spooner, for photograph and biography, please see this issue, p. 3408.

William A. Gardner, for photograph and biography, please see p. 3408.